Politecnico di Torino

Politecnico di Torino

Corso di Laurea Magistrale in Ingegneria Biomedica

A.a. 2020/2021

Sessione di Laurea Dicembre 2021

Radiobiological calculation for the treatment of patients in the field of FLASH radiotherapy

Relatori:
Prof. Gianni Coppa (DET)
Dott.ssa Faiza Bourhaleb (I-See s.r.l.)
Dott.ssa Claudia Pardi (I-See s.r.l.)

Candidata:
Antonietta Zema

Sommario

Il mio lavoro di tesi riguarda lo studio della radioterapia FLASH.
Recenti risultati in vivo hanno dimostrato che, nell'ambito della radioterapia, l'utilizzo di dosi ultraelevate (FLASH) rispetto alle dosi convenzionali (CONV) provoca un importante effetto benefico in termini di risparmio dei tessuti.
Al giorno d'oggi si stanno investigando diverse ipotesi per spiegare correttamente l'effetto FLASH. Tra le teorie più rilevanti vi è quella secondo cui questo effetto apparentemente benefico sia dovuto alle differenze di ossigenazione nei tessuti tumorali e sani.
La risposta differenziale tra FLASH-RT e CONV-RT potrebbe essere dovuta alla deplezione radiochimica dell'ossigeno a dosi molto elevate e alla conseguente radioresistenza conferita al tessuto irradiato. È ampiamente accettato che i tessuti ipossici sono più radioresistenti dei tessuti ben ossigenati. Questo perché in presenza di ossigeno molecolare c'è una fissazione del danno indiretto al DNA indotto dalle radiazioni.

A tal fine, sono stati realizzati diversi modelli sulla cinetica dell'ossigeno durante l'irradiazione per sviluppare un modello dipendente dal tempo sul comportamento dell'ossigeno. Questo modello mira ad analizzare, in termini di dose e dose-rate, l'aumento di ossigeno a causa della terapia.
A questo punto, appare evidente quanto sia importante modellare meccanicamente l'effetto dell'ossigeno nel processo di radiolisi dell'acqua per comprendere appieno il funzionamento della radioterapia FLASH. Tuttavia, a causa dei costi computazionali dell'interazione tra molti corpi, l'ossigeno è spesso ignorato nelle simulazioni con il metodo Monte Carlo comunemente effettuate.
Per rendere il codice MC ancora più versatile e applicarlo agli studi sull'Oxygen Enhancement Ratio (OER), è, allora, necessario includere più tipi di molecole, diverse dai radicali liberi generati dalla radiazione iniziale, nella simulazione della fase chimica.

A causa della complessità computazionale del problema "many-body" e della lunga durata della fase chimica, una simulazione passo dopo passo di questi processi sulle piattaforme computazionali della CPU può richiedere molto tempo. Per superare questi ostacoli, il calcolo parallelo basato su unità di elaborazione grafica (GPU) può essere

un'opzione conveniente. Un esempio è un toolkit di simulazione MC microscopica basato su GPU e open-source, gMicroMC.
Questo toolkit rappresenta lo strumento utilizzato durante il mio lavoro di tesi per eseguire simulazioni MC.
Quindi, lo scopo finale è quello di valutare la risposta della terapia FLASH alla variazione di parametri significativi a livello fisico e biologico.

Abstract

My thesis work concerns the study of FLASH radiotherapy.
Recent in vivo results have shown prominent tissue sparing effect of radiotherapy with ultra-high dose rates (FLASH) compared to conventional dose rates (CONV).
To nowadays several hypotheses are being investigated to correctly explain the FLASH effect. It has been suggested, among the most relevant theories, that this apparently beneficial effect is due to differences in oxygenation in tumor and healthy tissues.
The differential response between FLASH-RT and CONV-RT may be due to radiochemical oxygen depletion at very high doses and the resulting radioresistance conferred on the irradiated tissue. It is largely accepted that hypoxic tissues are more radioresistant than well-oxygenated tissues. This is because in the presence of molecular oxygen there is a fixation of radiation-induced indirect DNA damage.

To this end, several models on the kinetics of oxygen during irradiation have been realized to develop a time-dependent model on the behaviour of oxygen. This model aims to analyse, in terms of dose and dose-rate, the oxygen enhancement because of the therapy. At this point, it becomes apparent how important it is to mechanistically model the effect of oxygen in the water radiolysis process to fully understand how FLASH radiation therapy works. However, due to the computational costs of many-body interaction, oxygen is often ignored in simulations with common microscopic Monte Carlo tools.
To make the MC code even more versatile and apply it to Oxygen Enhancement Ratio (OER) studies, it is necessary to include more types of molecules other than free radicals generated by the initial radiation in the chemical phase simulation.

However, due to the computational complexity of the "many-body" problem and the long-time duration of the chemical phase, a step-by-step simulation of these relevant processes on conventional CPU computational platforms can be time-consuming. Under the constraint of computational resources, studies typically suffer from a narrow simulation region or short time duration, limiting their broad applications. To overcome these obstacles, Graphical Processing Unit (GPU)-based parallel computing can be a cost-

effective option. An example is an open-source, GPU-based microscopic MC simulation toolkit, gMicroMC.

This toolkit represents the tool used during my thesis work to perform MC simulations. So, the final purpose is to evaluate the response of FLASH therapy to the variation of significant parameters at physical and biological.

Un doveroso e sentito ringraziamento al mio relatore, il prof. Coppa.
Grazie per avermi dato la possibilità di mettermi in gioco,
grazie per la fiducia, il supporto e il tempo dedicatomi.
Grazie di cuore.

Grazie anche al gruppo di I-SEE, alla dottoressa Bourhaleb
per avermi insegnato a pensare fuori dagli schemi e a Claudia,
per avermi seguito durante tutto il percorso
e per aver sopportato me e i miei infiniti messaggi su WhatsApp.

Grazie ai miei amici, tutti, per essere semplicemente voi.

Grazie alla mia persona, Laura,
certi legami sfidano le distanze, il tempo e la logica. Tu sai.
E grazie a Teresa, è dai rapporti inaspettati che nascono i legami più forti.
Senza voi due, senza i vostri messaggi, le vostre chiamate
e le nostre uscite, tutto sarebbe stato più difficile.
Vi voglio bene.

Il ringraziamento più importante va alla mia famiglia,
non so dove sarei senza di voi.
E grazie a mio padre, per non aver smesso di credere in me
anche quando non ci credevo più nemmeno io.

Infine, grazie a chiunque, che sia per una stagione o per una vita intera,
abbia fatto parte del mio percorso.
A ognuno di voi devo qualcosa.

Table of contents

List of figures

List of tables

Chapter 1

1. Radiotherapy

1.1 Introduction

Radiotherapy is a medical therapy based on the use of ionizing radiation. It is mainly used in the treatment of cancer, in fact it uses a beam of penetrating photons, with 5-10 MeV of energy, to damage the genetic heritage of diseased cells and thus prevent them from proliferating. Radiotherapy can be curative in several types of cancer, if they are confined to one area of the body based on the TNM classification of the lesion itself.

This type of therapy is often combined with surgery, chemotherapy, hormone therapy, and immunotherapy. The purpose of treatment, whether curative-radical, adjuvant, neoadjuvant, therapeutic or palliative, depends on the type of tumor, location and stage, as well as the patient's overall health.

Ionizing radiations employed in radiotherapy can damage the DNA of the target tissue. Tumor cells are, in general, poorly able to repair their own damage and therefore undergo cell death by apoptosis. To spare healthy tissues, such as skin or organs that the radiation must pass through to reach the tumor, the radiation beams are directed from different angles, intersecting in the centre of the area to be treated, where therefore there will be a greater amount of total absorbed dose than that present in adjacent areas.

The advent of new technologies in diagnostic imaging, such as magnetic resonance imaging (MRI) in 1970 and positron emission tomography (PET) in 1980, led to the development of new ways to use radiation therapy. Examples include three-dimensional (3D) conformal radiation therapy, intensity-modulated radiation therapy (IMRT), image-guided radiation therapy (IGRT), and tomotherapy. These advances allow oncologists to better see and target tumors, with greater organ preservation and fewer side effects.

Radiotherapy, alone or in combination with surgery and/or chemotherapy, is, therefore, an effective tool for local tumor control. It is a well-established medical practice of proven efficacy, but it has contraindications in the potential dangers due to the use of ionizing radiation itself, in the possible damage from radiation and in the likelihood that the same induce the onset of secondary tumors.

The mechanism of interaction between the beam of photons exploited by radiotherapy and the diseased cells is as follows: x-ray photons strike electrons in the tissues and set them in motion. These, called secondary electrons, travel a centimetre or two into the tissues and ionize the atoms of the DNA molecules in the cells they encounter, thereby disengaging the functioning of their genes.
Two important radiotherapeutic modalities are TBI and TSEBI:

- Total Body Irradiation (TBI) is the total and simultaneous irradiation of the body (in one or more fractions) using high-energy photon beams. It consists of a particular radiotherapy technique used to prepare the patient to receive a bone marrow transplant (TMO or BMT). Depending on the needs, this type of intervention can be performed with high dose, low dose or very low dose administrations. Specifically, the aims of this treatment are twofold: to suppress the immune system to prevent rejection of the marrow of family or non-family donor, and to eradicate the neoplastic cells that remain after chemotherapy treatments.
- Total Skin Electron Beam Irradiation (TSEBI) is the total skin irradiation performed with electron beams. This therapy is used in the case of diffuse cutaneous neoplasms or in patients suffering from mycosis fungoides [1].

1.2 Working principles

Radiotherapy is based on the principle of directing ionizing radiation at cancer cells to damage their DNA. While healthy cells have mechanisms to repair damage that may occur to their DNA, cancer cells have much less efficient mechanisms, so damage is more likely to be lethal for this type of cell. Ionizing radiation generates in the cells free radicals, which damage the genetic patrimony of the host cell not able to oppose them.
The main limitation in the use of this technique is that the cells of solid tumors are in oxygen debt (hypoxia) and this makes them more resistant to radiation the less oxygen is present. Oxygen contributes to make less repairable the biological damage caused by free radicals generated by ionization and interacts with free hydrogen atoms H^+ creating oxidant OHx: this inhibits the return reaction that would otherwise occur (from Hx + OHx to H2O). This effect is more pronounced in low energy radiation (high linear energy

transfer), so that in the presence of oxygen the biological effectiveness of such radiation is increased by 3 times.

1.2.1 Treatment planning

Programmed procedures on radiotherapy machines include calibration of dosimetry systems and calibration of therapy beams. The first step in the patient procedure is to position the patient and to maintain the reproducibility of comfortable immobilisation accessories. A “pre-simulation x-ray” can then be carried out in which special lasers are used, using axial tomography, to identify the correct 'centring' coordinates. This makes it possible to obtain DRRs (or reconstructed digital X-rays), which are necessary to reconstruct a three-dimensional image of the treatment area and, therefore, to identify possible critical situations and/or those of clinical relevance.

With this data, a TPS (Treatment Planning System) is drawn up, which identifies the areas to be irradiated and the OARs (Organs At Risk, organs not to be irradiated or spared). TPS are mainly based on two processes:

- Forward Planning: the configuration of the beams (number, direction, fluence and energy) is varied manually until a dose distribution in accordance with the clinical prescription is achieved.
- Inverse Planning: based on the clinical prescription, the TPS has the task of and direction of the beams to obtain the dose distribution that best meets the distribution that best meets the prescription.

Ultimately, a TPS must be able not only to calculate the dose distribution as a function of beam configuration, but also to assess the biological impact associated with this distribution in the different organs involved. For this reason, each TPS has at its basis a radiobiological model of cellular inactivation aimed at assessing the effect of radiation on tissue.

1.2.2 Therapy goals

Depending on the type of tumour and the clinical condition of the patient, radiotherapy can be used with different objectives:

- Curative or radical radiotherapy: its aim is to completely eliminate the tumour;
- Preoperative or neoadjuvant radiotherapy: this is carried out before surgery to remove the tumour to reduce its size and make the operation easier. It is also used to reduce the risk that a small number of diseased cells may spread during surgery;

- Post-operative or adjuvant radiotherapy: this is prescribed after cancer surgery to increase the chances of eliminating any remaining cancer cells and preventing the disease from returning;
- Intra-operative radiotherapy, also known as IORT (Intra-Operative Radiotherapy): this involves administering a dose of radiation during surgery to remove the tumour. It requires special equipment and protection systems in the operating theatre and is therefore only performed in certain specialised centres;
- Palliative radiotherapy: the aim is to stop the growth of the tumour and alleviate its symptoms, including pain in advanced and metastatic forms, thus improving patients' quality of life;
- Total body radiotherapy: this procedure irradiates the patient's entire body to destroy the diseased cells in some particular cancers that affect the cells of the blood and lymphatic system, such as certain types of leukaemia or lymphoma. The affected cells are then replaced by new healthy blood or lymphatic cells through a transplant of bone marrow or particular progenitor cells, called stem cells;
- Ablative radiotherapy: here, high doses of radiotherapy are administered to small tumours; there are usually only a few treatment sessions (1 to 5) and stereotactic techniques are used [1].

1.3 Radiotherapy techniques

Radiotherapy can be administered in two ways:

- External or external beam radiotherapy: the source of the rays is positioned outside the body;
- Internal radiotherapy: radiation sources are placed inside the body near or in the tumour mass (brachytherapy), for example using applicators, and then removed. Radiotherapy sources are always sealed, i.e. they cannot enter the bloodstream and are not metabolised.

Contrary to common opinion, radiotherapy does not include what is known as radiometabolic therapy, which involves the administration of a radioactive liquid that is specifically absorbed by the tumour cells.

However, radiotherapy treatment is customised for each patient depending on the type of tumour, its size, location in the body and the patient's own condition. Therefore, there is no such thing as one radiotherapy treatment that is better or more effective than another. For example, when the volume of the tumour mass is large, as in the case of some lung or breast tumours, intensity-modulated radiotherapy is used, whereas for small volumes, as in the case of a brain tumour or a small metastasis, stereotactic radiotherapy is generally preferred. The aim is to apply the best available technique to each individual case.

1.3.1 Internal radiotherapy

In this case, radioactive metals (mostly iridium, caesium and palladium) are placed inside the tumour or very close to it, releasing radiation directly onto the tumour mass. The treatment is called brachytherapy (from the Greek *brachýs*=short) or also contact radiotherapy: in this case the radiation source is placed directly in contact with the target to be hit. In turn, brachytherapy can be divided into four forms:

- Interstitial brachytherapy: small radioactive sources are implanted in the tumour using a minimally invasive surgical procedure;
- Endocavitary brachytherapy: radioactive material is introduced into natural body cavities (e.g. oral cavity, uterus, oesophagus, bronchus) using special probes, so that it is close to the tumour;
- Contact brachytherapy: applicators with radioactive sources are placed on the skin; it is used in cutaneous neoplasms;
- Episcleral brachytherapy: this uses plates containing a radioactive source, shaped into different shapes and diameters; it is used to treat melanoma of the eye (uveal).

1.3.2 External radiotherapy

In external radiotherapy, high-energy ionising radiation (x-rays, cobalt gamma radiation, or beams of particles such as protons and electrons) is emitted by a device located outside the patient's body. This device, which does not come into direct contact with the body and does not cause any pain, directs the radiation to the precise location of the tumour tissue to be destroyed. It is used with both photon radiation and fast electrons.

It is referred to:

- Orthovoltage: low-energy X-rays from machines of about 50-500 kV.
- High-voltage: γ-rays or X-photons usually from 4 MV produced by a linear accelerator for radiotherapy.

Electrons have a different mode of dose spread from that of X-rays, since given the maximum dose at a depth that depends on their energy, the dose then goes very quickly to almost zero and are therefore used to irradiate more superficial tissues, sparing deeper ones. Some types of external radiotherapy are:

- Radiotherapy: this is an established treatment that delivers radiation to the tumour mass from different angles. The other types of radiotherapy described below have evolved from this.
- Three-dimensional conformal radiotherapy (or D-conformal radiotherapy or 3D-CRT). The radiation beam is shaped according to the shape and volume of the tumour mass, making it possible to use higher doses of radiation directed more precisely at the tumour, while surrounding healthy cells are exposed to lower doses and therefore with less risk of side effects. The definition of the target to be treated is based on computed tomography (CT), which provides a three-dimensional projection of the tumour.
- Intensity Modulated Radiation Therapy (IMRT) or intensity modulated beam therapy. This allows the radiation beam to be modulated, thus having beams of different intensities, and consequently to plan the highest dose to be directed at the target, i.e., the tumour, even in irregular shapes (e.g., concave), while sparing the surrounding healthy tissues. Tomotherapy falls into this category.
- 4D radiotherapy (4D-RT). It considers the movement of organs due to respiration and intestinal peristalsis during the radiotherapy session (hence the name "4D" i.e., 3D-CRT + time factor = 4D). It is extremely precise and saves a lot healthier tissue than other methods, because when 4D radiotherapy is not used, a wider margin around the tumour must be considered to account for the movement of the tumour mass itself due to the act of breathing.
- Adaptive radiotherapy. The radiotherapy plan is drawn up at each session to consider the anatomy of that day (day plan).
- Stereotactic Brain or Body Radiation Therapy (SBRT). It allows a high dose of radiation to be delivered to small tumours; it is a very accurate and precise technique that spares surrounding healthy tissue and therefore has many applications, for example in the treatment of prostate, lung, pancreatic cancer and metastases (brain, lung, liver).

Although there are some differences between one technique and another, the procedure is generally as follows: first the target, i.e. the position of the tumour, is defined by means of special diagnostic investigations and three-dimensional reconstructions; then, in order to protect the healthy parts, special customised shielding is used by means of blades (3D-conformal radiotherapy) or dose modulation (intensity-modulated radiotherapy) inside the device; these then allow the radiation beam to be directed in the desired way [1].

1.4 Hadrontherapy

In external radiotherapy, protons, neutrons and carbon ions are used for hadrontherapy. The name is derived from hadron therapy because it is a therapy using beams of hadrons, i.e., particles characterised by strong interaction. The tumour-killing effect of hadrontherapy is greater because the hadrons act deeper and are able to deposit high doses of radiation in the tumour while limiting doses to critical organs, even when these are very close to the target. Hadrontherapy involves the use of a cyclotron to accelerate particles to high speeds that are impossible to achieve with linear accelerators.

1.4.1 Working mechanisms of Hadrontherapy

Hadron therapy works by targeting the tumour with ionising particles. These particles damage the DNA of tissue cells, causing them to die. Because of their reduced ability to repair damaged DNA, cancer cells are particularly vulnerable to these attacks.

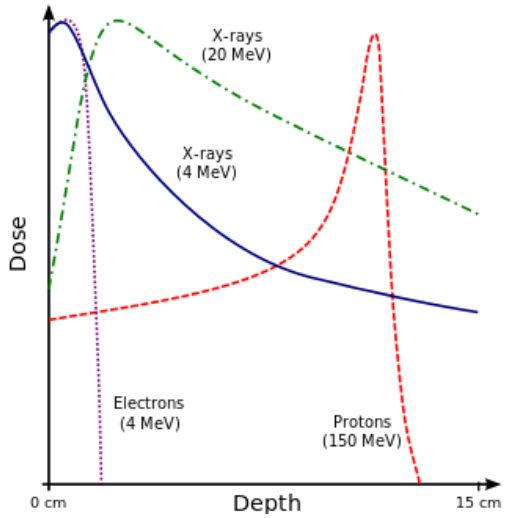

Figure 1.1: Comparison of electrons, protons and x-rays [2].

As can be seen from Figure 1.1, beams of electrons, x-rays of different energy and protons penetrate human tissue in different ways. The path taken by electrons is very short and they are only useful in areas close to the skin. X-rays penetrate more deeply but the dose

absorbed by the tissue has a typical exponential decay with increasing thickness. For protons and heavier ions, on the other hand, the dose increases with increasing thickness until the Bragg peak, which occurs just before the end of the journey. After this peak, the dose drops to zero (in the case of protons) or almost zero (in the case of heavy ions). The advantage is that less energy is deposited in the healthy tissue surrounding the target tissue, saving it from unnecessary damage.

The ions are first accelerated by means of a cyclotron or synchrotron. The final energy of the emerging particle beam defines the penetration depth, and thus, the position where the maximum dose will be delivered. Since it is easy to deflect the beam by means of electromagnets in a transverse direction, a raster scanning method can be used, i.e., scanning the area of the target volume as in a cathode-ray tube. If, in addition, the beam energy and thus the penetration depth is varied, a whole target volume can be divided into three dimensions, providing exact irradiation following the shape of the tumour. This is one of the great advantages over conventional x-ray therapy systems [2].

So, hadrontherapy offers some significant advantages such as:

- Ability to treat radioresistant tumors: the mechanism of energy release for hadrons causes a large amount of breakage in chemical bonds present in biological macromolecules, particularly DNA.
- Precision of treatment and preservation of healthy tissue: the release of energy, and therefore the destruction of cells, is extremely selective. This means that only tumor cells are affected with a high intensity, while healthy tissues are spared. This phenomenon is made possible by the way the energy is released during treatment, when the accelerated particle beam reaches the patient's body, it is so fast that it cannot interact with the tissues and therefore doesn’t damage them. However, the beam undergoes a progressive slowdown until it reaches a point where it stops. At this point, located exactly where the tumor is, all the residual energy of the particles is released and the maximum tissue damage occurs. This one is called "Bragg Peak". Due to the physical properties of hadronic particles, the particle beam does not scatter, remains collimated, as it passes through the patient's body and thus further minimizes damage to surrounding healthy tissue.

This structure clearly shows how the use of charged particles allows to drastically reduce the dose deposited in the healthy tissues crossed by the radiation in the case of tumors located deep, thus limiting the onset of complications related to radiation damage.
The combination of the hadrontherapy advantages, with a very high personalization of the treatment in each phase, involves a remarkable destructive efficacy on tumor tissues. For this reason, the target must be positioned with millimetric precision, much higher than in traditional radiotherapy [4-8].

1.4.2 Proton therapy

Proton therapy is a type of hadrontherapy that uses a beam of protons to irradiate diseased biological tissue, often in the treatment of cancer. The main advantage of proton therapy is its ability to localise the dosage of ionising radiation more precisely than other types of external radiation therapy. However, there is not yet completely certain evidence whether this constitutes an overall advantage over other, less expensive treatments.

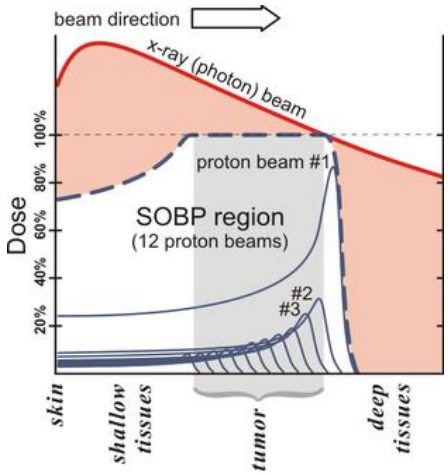

Figure 1.2: Energy pattern in a typical proton therapy treatment [3].

Because of their relatively large mass, protons have little lateral dispersion when crossing tissues; the beam therefore does not spread very far, remaining rather focused on the tumour mass and thus ensuring only low side effects to the surrounding tissues. All protons of a given energy have a given penetration power and therefore very few protons penetrate beyond this distance, sparing the tissues behind the tumour. In addition, the dose delivered to the tissue is maximum only in the last few millimetres of the particle's path (the maximum point is the Bragg peak).
To treat tumours at greater depths, the proton accelerator must produce a beam with a higher energy, usually measured in eV. If, on the other hand, it is necessary to treat

tumours closer to the surface of the body, protons of lower energy can be used. Accelerators used for proton therapy typically produce protons with energies in the range of 70-250 MeV. By adjusting the energy of the protons during the treatment, the tissues before and after the tumour mass can be spared more, concentrating the maximum energy on this mass. In most treatments, protons of different energies and Bragg peaks at different depths are applied to treat the entire tumour. The total radiation dose of the protons is called the spread-out Bragg peak (SOBP). It is important to understand that, while tissues behind the tumour receive almost no radiation from proton therapy, tissues in front of or shallower than the tumour receive a radiation dose based on SOBP [3].

1.5 Dose fractionation

Radiotherapy, like pharmacotherapy, obviously has biological effects and the total dose, delivered and absorbed, is also important in relation to the chosen fractionation, which correlates with the concept of dose delivered over time. In fact, external radiation treatment is usually not continuous, but fractionated, and is performed according to two main dose delivery schemes:

- conventional: therapy is carried out with no more than one daily fraction;
- hypofractionated: therapy is also performed with no more than one daily fraction;
- hyperfractionated: therapy is performed with more than one daily fraction, usually no less than six hours apart.

Parameters such as dose fractionation, irradiated volume and total delivered dose are partly related to toxicity and local control of radiotherapy treatments with dosimetry and radiobiological optimisation. The method of administering small and frequent doses is often used to allow healthy cells and tissues to repair radiation-induced damage, without altering the efficacy on the tumour.

1.6 Side effects

Radiotherapy is a painless method of treatment. In cases where palliative treatment is used, it also has minimal side effects. In cases where radical treatments are used, various types of side effects may occur during or weeks after treatment (early side effects) or in the months or years directly following treatment (late side effects).

The nature of the side effects depends on the organ treated, the fractionation, the dose rate, the total treatment time, the treatment intervals, the volume irradiated and the type of technique used. Side effects are divided into acute and chronic.
Main acute side effects are:

- Leukopenia;
- Epithelial tissue damage (radiodermatitis and early mucositis);
- Inflammation and oedema of the irradiated area;
- Fatigue.

Chronic side effects may be minimal and depend on the tissue receiving the treatment. The main ones are:

- Late-onset radiodermatitis and fibrosis;
- Loss of hair in irradiated areas;
- Dry mouth;
- Secondarily radio-induced or chemoradiation-induced tumours;
- Spinal cord injury (rare, and usually cervical and thoracic);
- Infertility;
- Radio-necrosis.

Chapter 2

2. Radiobiology

2.1 Introduction to radiobiology

Radiobiology is the science of evaluating and modelling the effect of radiation on biological tissues, whether healthy or cancerous. The term *biological effect* refers to the probability of cell survival associated with a given dose level. The radiation, in fact, can be effective depending on the tissue irradiated, as each tissue is characterized by a different radiosensitivity. To model the biological response to ionizing radiation are performed in-vitro experiments in which it is evaluated the progressive loss of clonogenicity of cells as a function of the dose administered. The results of each experiment are summarized in an experimental curve called survival curve.

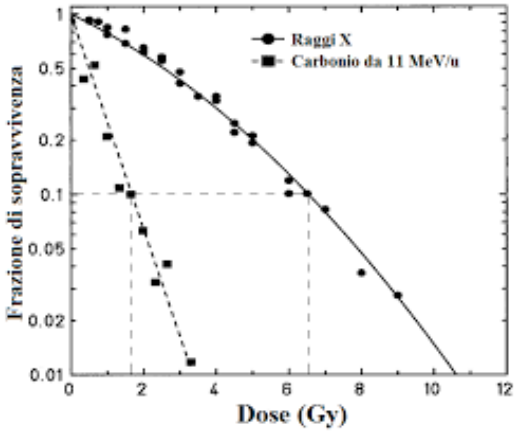

Figure 2.1: Example of experimental survival curve [9].

Radiation is classified into two main categories:

- Non-ionizing radiation (cannot ionize matter);
- Ionizing radiation (can ionize matter).

There are major categories of ionizing radiations:

- Directly ionizing radiation, charged particles such as electrons, protons, alpha particles that deposit dose right away;

- Indirectly ionizing particle, neutral particles such as photons, neutrons that interact with charged particles that deposit dose.

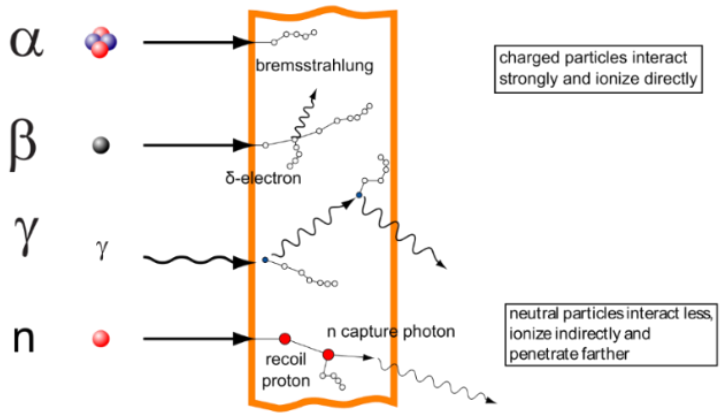

Figure 2.2: Interaction of ionizing radiations with matter [11].

If radiation is absorbed in biological material, ionizations and excitations occur in a pattern that depends on the type of radiation involved. Depending on how far the primary ionization events are separated in the space, radiation is characterized as sparsely ionizing (x-rays) or densely ionizing (α-particles). Havier particles with larger charge produce higher ionization density and, for a given particle type, the density of ionization decreases as the energy and velocity go up.

2.1.1 Effects of non-ionizing radiation

Non-ionising radiation is defined as radiation that is not capable of producing ionisation in materials exposed to it. Non-ionising radiation includes all non-ionising radiation, starting with ELF (Extremely Low Frequency). In recent years there have been increasing questions about radio frequency (RF) and microwave (MW) fields.

The units used to express the magnitude of exposure to RF and microwave fields are the volt/meter (V/m) for the strength of the electrical component E of the field, the ampere/meter (A/m) for the strength of the magnetic component H of the field, and the watt/m² (W/m²) for the density S of radiated power. The specific energy absorption rate (SAR) is usually measured in W/kg.

Other units include the gauss and tesla. The gauss (symbol G) is the unit of magnetic flux density (or magnetic induction) in the electromagnetic CGS system. One gauss is equal to 1 maxwell per square centimetre. The relationship between the gauss and the tesla (symbol T), the corresponding unit of measurement in the SI system, is: 1T=10 000 G; 1G = 0.0001 T.

2.1.2 Effects of ionizing radiations

Ionizing radiation, the most important from the point of view of application, is radiation with sufficient energy to cause ionisation of the atoms it encounters.

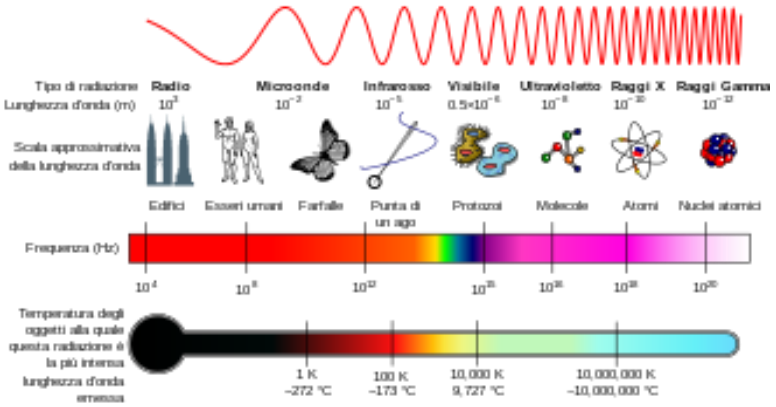

Figure 2.3: Electromagnetic spectrum [13].

Conventionally, radiation with a frequency greater than $3*10^{15}$ Hz is considered ionizing. Energy is measured in joules or electron volts (eV). The most used unit of measurement is the Gray (Gy), i.e., the dose of energy absorbed per unit mass; the LET, the linear energy transfer, is the energy released by the radiation per unit length; and for biological tissues, from the point of view of application, including radiation protection, the unit of measurement is the sievert (Sv). The becquerel (symbol Bq) is the International System unit of measurement for the activity of a radionuclide and is defined as the activity of a radionuclide that has one decay per second. It is therefore dimensionally equivalent to the inverse of time. 1Bq is equivalent to 1 disintegration per second, equivalence to older units such as curie (Ci).

To ionise matter, the radiation must have sufficient energy to interact with the electrons of the atoms it encounters. Charged particles can interact strongly with matter, so electrons, positrons and alpha particles can ionise matter directly. Photons and neutrons, on the other hand, although not charged, can ionise matter if they have sufficient energy (photons with a frequency equal to or greater than ultraviolet rays are considered ionising for humans).

The interaction of photons with matter can produce, as the energy increases, the photoelectric effect, the Compton effect and the production of couples.

Ionizing radiation can have an indirect effect on organic matter through radiolysis of water and the resulting formation of free radicals. Water, for quantitative reasons, is the

molecule with which an interaction of the ionising particle takes place almost constantly. Radiolysis takes place according to these steps (energy = hν, where h is Planck's constant and ν is frequency):

- $h\nu + H_2O \rightarrow H_2O^+ + e^-$
- $e^- + H_2O \rightarrow H_2O^-$
- $H_2O^+ \rightarrow H^+ + OH^\circ$
- $H_2O \rightarrow H^\circ + OH^-$

In the absence of O_2, the radicals will interact with each other in all possible combinations to produce H_2O, H_2 and H_2O_2. If O_2 is present in the irradiated medium in sufficient concentration, H-radicals are captured, resulting in the formation of the highly oxidising HO_2 radical:

- $O_2 + H \rightarrow HO_2$
- $HO_2 + e^- \rightarrow HO_2^-$
- $HO_2^- + H^+ \rightarrow H_2O_2$
- $H_2O_2 + 2H \rightarrow 2H_2O$

This would explain how, in biological substrates, the effect induced, radiation being equal, is about 2-3 times greater in the presence of O_2 (oxygen effect). In the progressive growth of a tumour focus, the production of a newly formed network of vessels is always more or less insufficient in relation to the extent of neo-production of tumour cells. The distance at which many of these cells are located from the capillary wall may mean that they are inadequately supplied with O_2 by diffusion. These hypoxic or anoxic cells are not very radiosensitive. Radiation with a low LET (Linear energy transfer) such as photons (and electrons) have a radiobiological action influenced by the presence of oxygen. (High-LET radiation: protons, neutrons, heavy particles have a radiobiological action unaffected by the presence of oxygen).

The chemical and biochemical effects that ionising radiation can have include bond breaking, molecular alterations, damage to the cytoplasm, RNA and DNA.

DNA damage can take the form of chain breaks, alterations to bases, destruction of sugars, formation of cross-links. DNA damage, if not properly repaired and transcribed, leads to a series of chromosome and/or chromatid aberrations. Such damage, if not amenable to cellular repair, can lead to cell death. If this does not occur, the damage can mutate the

cell and the resulting biological effects are only morpho-functional and metabolic alterations, lesions of genetic material, aberrations of various cellular components, uncontrolled cell growth and angiogenesis.

It is worth mentioning modelling, which studies mathematical formulations to interpret and predict the effects of radiation [9-13].

2.1.3 Linear Energy Transfer

So, to define the quality of ionizing radiation beam, it is used the Linear Energy Transfer LET. LET of charged particles in a medium is the quotient of dE_L by dl, where dE_L is the average energy locally imparted to the medium by a charged particle of specified energy in traversing a distance dl.

(2.1)

$$LET = \frac{dE_L}{dl}$$

The term locally imparted may refer either to a maximum distance from the particle track or to a maximum value of discrete energy loss by the particle beyond which losses are no longer considered as local. In either case, the limits chosen should be specified. Its unit is KeV/µm and it is an average quantity, typically track averaged.

Radiation	***LET (KeV/ µm)***
250 kVp x-rays	2
Cobalt-60 rays	0.3
3 MeV x-rays	0.3
1Mev electrons	0.25

Tab 2.1 : Typical LET values for commonly used

Optimal LET is ≈ 100 KeV/µm in terms of producing a biological effect. At this density of ionization, the average separation in ionizing events is equal to the diameter of DNA double helix which causes significant double strands breaks, that are the basis of most biological effects [14].

More in detail the LET is obtained from the Bethe-Bloch relation (it is the formula that, considering heavy charged particles describes the dominant process, that is the coulombic interaction between radiation and atomic electrons that causes excitation and ionization of the atoms of the material):

(2.2)

$$-\frac{dE}{dl} = 4\pi N_A {r_e}^2 m_e c^2 \rho \frac{Z}{A}\frac{z^2}{\beta^2}\left[\frac{1}{2}\ln\left(\frac{2m_e c^2 \beta^2 \gamma^2 T_{max}}{I^2}\right) - \beta^2 - \frac{\delta}{2}\right]$$

in the limiting case where $T_{max} \rightarrow +\infty$, i.e., not placing an upper limit on the amount of energy that can be transferred to an electron in a single collision. The LET has a large dependence on the type of particle considered and its energy, in fact in figure 2.4 it shows the variations of LET as a function of energy for different types of ions.

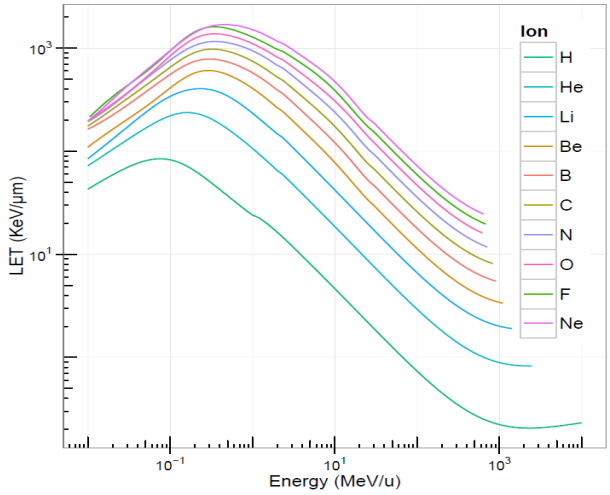

Figure 2.4: Variation in LET for different types of ions [15].

It can be observed that the LET increases as the mass of the ion increases, for this reason with the term high LET radiation it refers to heavy ions. It can also be observed a strong dependence on the energy of the radiation under examination: in particular, excluding the extreme regions where the trend is reversed, there is a relationship of inverse proportionality between LET and energy for which a high energy corresponds to a low LET and vice versa [15].

2.2 Relative Biological Effectiveness

Absorbed dose can be a poor indicator of the biological effect of radiation. Biological effects can depend on many other factors such as type of radiation, initial energy and type of tissue. For example, 1 Gy of neutrons produces a greater biological effect than 1 Gy of x-rays due the difference in the pattern of energy deposition. For this reason, it is introduced a new parameter, called Relative Biological Effectiveness RBE, that is the

ratio of biological effectiveness of one type of radiation relative to another, given the same amount of absorbed energy. RBE is an empirical value and varies:

- Type of ionizing radiation, energies involved;
- Biological effects such as cell death and oxygen tension.

RBE compares test radiation r with 250 kV x-rays is defined:

(2.3)

$$RBE = \frac{D_{250kV}}{D_r}$$

With D_r absorbed dose of radiation of type r that causes the same amount of biological damage as D_{250kV}.

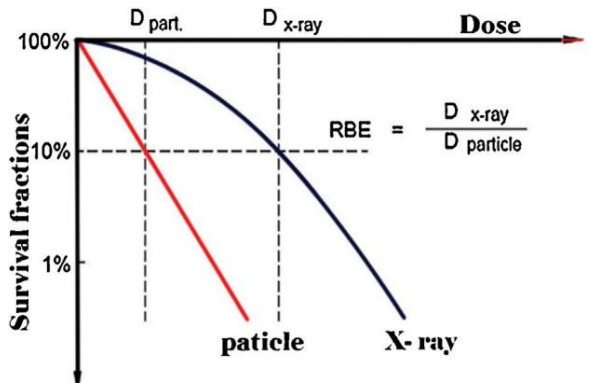

Figure 2.5: RBE definition [15].

In general, the RBE increases with LET to reach a maximum RBE of 3 – 8 (depending on the level of cell kill) at LET ≈ 100 KeV/µm and then decreases because of energy overkill [14].

2.3 Effect of interaction between ionizing radiation and biological systems

The potency of radiation is in its concentration and the damage done to the genetic material of each cell. In fact, the irradiation of each biological system generates, at the level of DNA, a succession of events that can be divided into consecutive temporal phases. These effects are evident both at the level of neoplastic tissues (tumor cells that escape the control mechanisms of proliferation and follow their own autonomous program of reproduction) and healthy tissues surrounding the tumor and that are inevitably exposed to radiation.

The effect can be divided in different phases: physical, biochemical, chemical and biological phase.

Physical phase

The physical phase is the one immediately following the radiation-matter interaction processes that cause excitation and/or ionization processes, and thus accompany the transfer and absorption of radiation into matter. This phase is of very short duration (about 10^{-8} seconds). The interaction modes depend mainly on the nature of the radiation and its energy. For example, corpuscular radiation collides directly with orbital electrons or, less frequently, with nuclei. In both cases there is the transformation of the atom into a charged ion. Electromagnetic radiation, instead, interact with atoms with four different mechanisms, depending on energy: photoelectric effect, Compton effect, couple effect and nuclear photodisintegration. For energies used in the medical field and for the Z of absorbing materials (biological tissues) the first two effects are predominant.

Secondary radiation (usually electrons) generated can, in turn, give rise to a chain of further interactions with other atoms if sufficiently energetic until it is completely dissipated their energy. Ionization phenomena in irradiated matter are not distributed homogeneously: they are conditioned by the nature and energy, as well as by the characteristics of the irradiated biological material.

Biochemical - Chemical phase

This one, with a duration of 10^{-3} seconds, consists in the production of modifications of the chemical structure of the molecular species of the irradiated biological system. The action can be direct or indirect:

- *Direct action*: radiation interacts directly with the critical target cell. Atoms of the target itself may be ionized or excited through Coulomb interactions leading to the chain of physical and chemical events that eventually produce the biological damage. It is a dominant process in the interaction of high LET particles such as neutrons or alpha particles with biological material.
- *Indirect action*: radiation interacts with other molecules and atoms. Within the cell free radicals are produced and, through diffusion, they damage the critical target. Indirect action can be modified by chemical sensitizers or radiation protectors.

Based on the enzymatic repair capabilities of DNA, it is possible to distinguish damage into:

- Non-reparable damage: lethal damage leading to cell death;
- Repairable damage:
  - potentially lethal but repairable by enzymatic systems;
  - Sublethal damage that does not result in cell death.

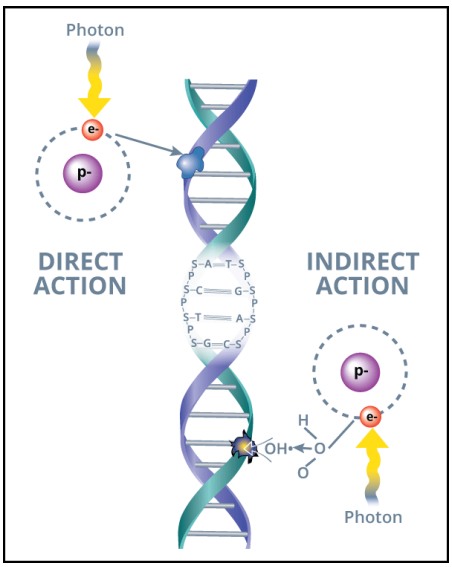

Figure 2.6: Action of radiation in cell damage [16].

Biological phase

The clinical manifestation (clinically detectable effect) of the biological effect of radiation always occurs at a certain distance from exposure (latency time).

The term acute effects is used to indicate the effects that occur days after a single exposure or during a fractionated irradiation, instead late effects is used to indicate effects that occur months or years after irradiation.

Some tissues respond with acute effects and late effects, others show only late effects.

The biological effect is expressed in cell killing or cell transformation (carcinogenesis and mutations). The primary target of radiation is DNA molecules, suffering breaks in chemical bonds. Depending on the extent of damage, it can be repaired through several repair mechanisms in place in a living organism [16].

Post radiation, the mechanisms of cell death are:

- *Mitotic death*: cells die attempting to divide, primarily due to asymmetric chromosome aberrations (most common mechanism);
- *Apoptosis*: it is programmed cells death, characterized by a predefined sequence of events resulting in cell separation in apoptotic bodies;
- *Bystander effect*: cells directly affected by radiation release cytotoxic molecules inducing death in neighbouring cells. [17]

The chronology of events following radiation exposure is shown in Table 2.2:

Phase	***Time***	***Main effects***
Physic phase	10^{-8} seconds	Ionization or excitation
Chemical phase	10^{-3} seconds	Formation of free radicals and peroxides
Biochemical phase	Seconds – minuts	Inactivation of enzymes and cellular organelles
Biological phase • damage repair • cell death	 24h Days – weeks	Inactivation, repair, cell and tissue death
Clinical phase • acute effects • late effects	 Days – weeks Months – years	Clinical manifestations in the organism

Tab 2.2: Temporal succession of events following irradiation.

2.4 LQ linear quadratic model

The radiobiological problem is to develop a parameterization that describes the probability of cell survival based on experimental observations for each tissue to each tissue and about the different irradiation conditions, with the purpose of to identify the radiobiological parameters that define the radiosensitivity and through which it is possible to evaluate the biological impact of radiation.

Several radiobiological models have been developed with the common intent to define an adequate parameterization for the survival curve. Among such models [18-22], the most used is the linear quadratic model LQ in which the shape of the survival curve is expressed by the relation:

(2.4)

$$S = e^{-\alpha D - \beta D^2}$$

or similarly, in logarithmic form:

(2.5)

$$\ln S = -\alpha D - \beta D^2$$

With:

- S the survival,
- D the administered dose,
- α and β and beta the radiobiological parameters defined by the linear quadratic model.

The survival S, in this case, assumes a probabilistic connotation: it is in fact defined as the probability of not observing lethal events in the cell after the irradiation process. This quantity is evaluated by means of the Poissonian statistic according to which the probability of observing n events is given by the following formula:

(2.6)

$$P(n) = \frac{e^{-\mu}\mu^n}{n!}$$

where μ indicates the mean value of the Poissonian.
The probability of not observing lethal events in the cell is therefore reduced to the expression:

(2.7)

$$S = \exp(-N_{leth})$$

Specifically, the linear quadratic parameterization evaluates the average number of lethal events per cell through the expression:

(2.8)

$$N_{leth} = E = \alpha D + \beta D^2$$

This quantity is also called *effect* and is often used to compare treatments of different types. It is in fact evaluated the *isoeffect dose*, that is the dose necessary to obtain a certain effect for each of the treatments compared. From the combination of the last two

expressions (2.7) and (2.8) derives, therefore, the linear square equation used for survival curves (2.4).

It is also possible to assign radiobiological significance to the different terms in the equation. The idea is that, because of interaction with radiation, the cell can suffer two types of damage: lethal or sublethal. Sublethal damage can be repaired by the cell or can combine with each other giving rise, in turn, to lethal damage and therefore no longer repairable. In the shape of the survival curve this manifests itself in a linear component ($-\alpha D$), associated with the occurrence of single lethal events following of the interaction of the cell with the radiation, and a quadratic component ($-\beta D^2$) associated with the possible combination of unrepaired damage resulting from the interaction of the cell with two different particles. These components are by nature stochastic, in particular the quadratic component assumes an additional level of stochasticity linked to the temporal dimension, since with the passage of time the probability increases that the sublethal damages are repaired by the cell and thus decreases the probability that these combine with each other. For this reason, only the quadratic component is sensitive to the temporal structure of the dose release and, therefore, the beta parameter will be of fundamental importance in assessing its effects.

Since survival identifies an average value per cell, this magnitude is well defined only in the case of low-LET radiation. In fact, using ions, i.e., radiation at high LET, one obtains a reduced number of particles with high ionization density resulting in a variable cellular configuration cellular variable in relation to the topological condition of the irradiation.

2.5 Ratio α/β

Radiotherapy has traditionally been a fractionated treatment course spread over several weeks. It takes advantage of differential repair abilities of normal and malignant tissues.

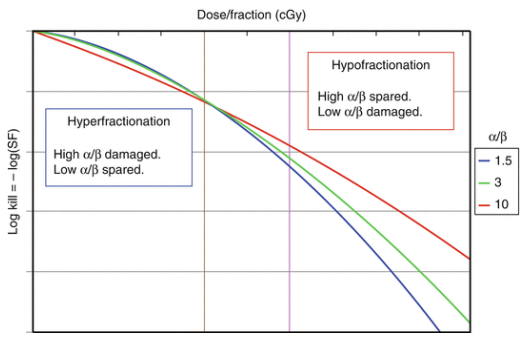

Figure 2.7: Fractionation [23].

The shape of the survival curve, according to the linear quadratic description, is defined exclusively by the value assumed by the radiobiological parameters α and β. Their ratio:

(2.9)

$$R = \frac{\alpha}{\beta} = \frac{[Gy^{-1}]}{[Gy^{-2}]} = [Gy]$$

The formula represents the dose value for which the quadratic component balances the linear one and is a way to characterize in a synthetic way the response of biological tissue to the radiation. For high values of R it expects a low sensitivity to the temporal effect and vice versa. Experimentally it can be observing a strong dependence of the parameters α and β on the type of particles used and the LET of the radiation under investigation. There is a progressive linearization of the curve as the LET of the particle increases, so the value of the ratio α/β tends to increase. Parallel to the linearization of the curve it can also observe an increased sensitivity of the tissues to radiation identified by an increase of α and a simultaneous decrease in the value of β, the consequence of which is a progressive loss of sensitivity to the temporal structure.

The dependence of α and β on the LET implies in turn a sensitivity of the radiobiological parameters to the type of radiation used and to the energy of the ion. Thus, given the type of radiation and the energy of the particle, the ratio α/β becomes characteristic and tissue-identifying, so different biological tissues respond to the radiation in a different way, in particular tissues characterized by high values of α/β are more radiosensitive and are less affected by the temporal structure of dose deposition.

So, ratio α/β gives the dose at which the linear and quadratic components of cell killing are equals. Use α/β ratios to generate treatment schedules employing different-sized doses per fraction to match the probability of causing a tissue injury. The values of the ratio α/β tends to be:

- Larger (≈ 10 Gy) for early-responding tissues and tumors;
- Lower (≈ 2 Gy) for late-responding tissues and tumors.

Fractionation has a profound effect on cell survival curves for low LET radiation (some for high LET). The main objective clinically is sparing of the normal tissue by giving it time to repair sublethal damage. Typically normal tissue repair mechanisms are much more effective than those of cancer cell's. So, it's necessary calculate the Biological

Equivalent Dose BED that indicate quantitatively the biological effect of any radiotherapy treatment, taking account of changes in dose-per-fraction or dose rate, total dose and overall time [23].

(2.10)

$$BED = nd(1 + d/[\alpha/\beta])$$

With:

- n number of fractions;
- d dose/fractions.

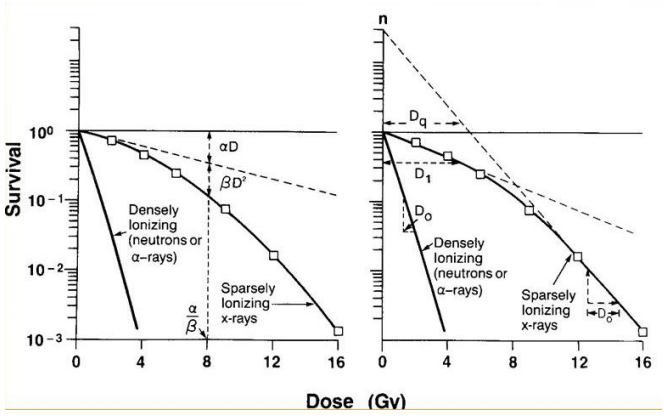

Figure 2.8: Ratio Alpha/Beta [24].

The fundamental principle on which radiotherapy is based is the need to maximize the treatment response of tumor tissue while minimizing damage to surrounding healthy tissue. In radiobiological terms, we define the probability of tumor control (TCP) as [24]:

(2.11)

$$TPC = \exp\left[-N_0\, exp\left(-\alpha D - \frac{1}{N}\beta D^2\right)\right]$$

Where:

- N_0 represents the initial number of clonogens;
- The internal exponential represents survival following a total dose D administered in fractions of d Gy per fraction.

The probability of observing complications in healthy tissues (NTCP) [26], is given by the following relationship:

(2.12)

$$NTCP = \frac{1}{\sqrt{2\pi}} \int_{-\infty}^{u(D,V)} \exp\left(-\frac{1}{2}x^2\right) dx$$

Where the dose and volume dependence is contained in the upper limit of integration:

(2.13)

$$u(D,V) = \frac{D - D_{50}(V)}{mD_{50}(V)}$$

The distance between the TCP and NTCP curves, identified in the size:

(2.14)

$$P^+ = TPC - NTCP$$

P^+ represents the so-called therapeutic window.

In general, the goal in developing a treatment plan is to maximize the therapeutic window. A first solution is, precisely, to fractionate the total dose giving time to healthy tissues to recover between a fraction and another and repair the damage suffered.

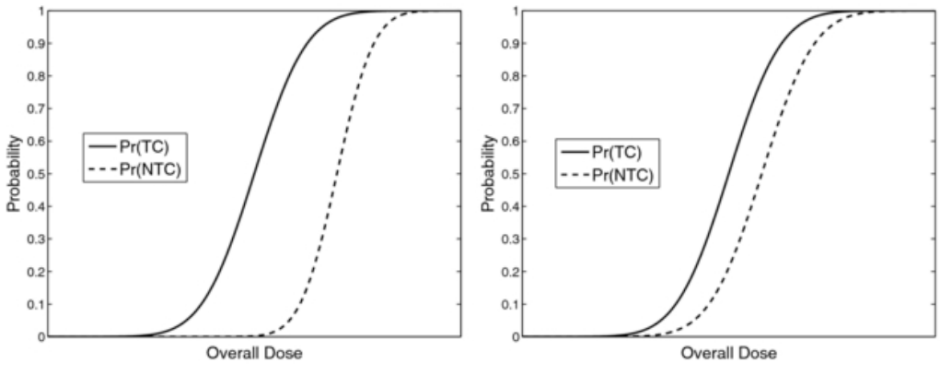

Figure 2.9: TCP and NTCP curves obtained in the case of acute (right) and fractionated dose (left [24]).

The figure 2.9 shows how fractionating the total dose allows to widen the therapeutic window.

2.6 Fractionation

Knowing and understanding the differences that characterize the temporal response to treatment of different types of biological tissue becomes essential to define and optimize the dose fractionation scheme.

Dose fractionation has always been a critical topic in radiotherapy, despite this to date a standard treatment plan involves the administration of daily fractions of 2 Gy; this dose value is considered the reference for each type of fractionated treatment. Therefore, it is called *hypofractionation* a treatment that involves the administration of one dose per fraction higher than 2 Gy, vice versa it speaks of *hyperfractionation* to indicate any treatment that provides a dose per fraction with a dose per fraction lower than 2 Gy. This implies that, for the same total dose total dose, a hypofractionated treatment will have a lower number of fractions compared to the standard standard treatment, vice versa for a hyperfractionated treatment.

At the mathematical level, what you do is compare the α/β ratio between tumor tissue (T) and healthy tissue (NT) involved in therapy. When:

(2.15)

$$\left(\frac{\alpha}{\beta}\right)_T > \left(\frac{\alpha}{\beta}\right)_{NT}$$

It means that the tumor has a lower sensitivity to fractionation than healthy tissue and that a hyperfractionated treatment should be chosen, because the ability of the tumor to repair the damage done is lower than that of healthy tissue.

Similarly, in the opposite condition:

(2.16)

$$\left(\frac{\alpha}{\beta}\right)_T < \left(\frac{\alpha}{\beta}\right)_{NT}$$

Hypofractionated treatment will be the choice, as the tumor benefits more from recovery time than healthy tissue.

There is also another type of fractionation, which has recently returned to the attention of the scientific community and it is *accelerated fractionation*. It is characterised by single fractions of 1.5-1.6 Gy. The total dose is not different from that of standard fractionation, but the total delivery time is significantly shorter. This fractionation aims to have fewer cells to be inactivated to obtain, for the same dose, a higher probability of curing the lesion. Since the total duration of treatment does not lead to the development of late damage, theoretically this type of fractionation should lead to a therapeutic gain. Reducing the total duration of treatment without reducing the total dose should increase

the therapeutic ratio, as long as the acute reactions are considered tolerable for the patient. However, by reducing the total duration of treatment it is necessary to reduce the total dose administered to prevent excessively severe acute reactions.
In this situation a therapeutic gain is achieved only if the dose reduction required to control acute side effects is not such that the acute side effects is not sufficient to allow neoplastic regeneration [25].

2.7 The four Rs of radiobiology

Fractionation of the radiation dose typically produces better tumor control for a given level of normal tissue toxicity than a single large dose. The basis for fractionation are:

- Repair of sublethal damage to cell between fractions caused by radiations (few hours);
- Reassortment of cells into radiosensitive phases of cycle (few hours);
- Repopulation or regrowth of cells between fractions (5-7 week);
- Reoxygenation of hypoxic cells to make them more sensitive to radiation (hours to few days).

Repair

Radiation generates highly reactive oxygen species (hROS) from water molecules. They are short-lived and rapidly interact with biomolecules in cells. Those that are generated within 2 nm of the DNA are more important in causing DNA damage.
Repair deficient cells (e.g., ATM) are exquisitely sensitive to ionizing radiation. Differential repair abilities affect α/β ratio.
The ability to recover from sublethal damage is a function of cell type and in healthy tissues is highly variable. The ability to recover from sub-lethal damage is variable even in tumors, but it is generally lower than in healthy tissues of origin. Repair of life-threatening damage occurs in similar time frames; its importance is conditioned by the tissue proliferative kinetics.

Reassortment

Cells exhibit differential radiation sensitivity while in the different phases of the cell cycle. Cells in mitosis are most sensitive to DNA damaging agents and cells in late S-

phases being most resistant. With multiple doses, cells progress through to a new phase of the cell cycle. Sensitization due to re-assortment causes therapeutic gain.

Repopulation

Damage and cell death occur during the treatment may induce an increased rate of cell proliferation. It is most important in early-responding normal tissue, but it is also true for tumors as well.

An irradiated cell population can respond to radio-induced damage by increasing cell proliferation cells. Repopulation is evident in healthy tissues with rapid kinetics and reduces the extent of damage, it is scarce in tissues with a slow proliferation. In tumors with high proliferative kinetics, it may reduce the efficacy of treatment. Tumor repopulation is most evident toward the end of fractionated radiation treatment; therefore, an excessive prolongation of treatment or the existence of interruptions may reduce the efficacy of therapy.

Reoxygenation

In tumors, the percentage of hypoxic cells is high (10-20%) and is due to the excessive distance from the vessels blood vessels or from alterations in blood flow. Dose fractionation tends to reduce hypoxia in the tumor, thus reducing the surviving population (i.e., the tumor mass) and improving the blood flow, with consequent increase in radiosensitivity of tumor cells.

The first component of reoxygenation, which is complete in several hours, is due to the reoxygenation of acutely hypoxic. These cells are hypoxic at the time of irradiation because they are in an area near a temporarily occluded blood vessel and they are reoxygenate rapidly when the vessel reopens. Tumor cell death due to irradiation results in a reduction in tumor volume. Those tumor cells that were outside the range of oxygen diffusion come to be closer to the vessels and reoxygenate. This slow component of reoxygenation takes days to manifest and involves the reoxygenation of chronically hypoxic cells [27].

Repair and Repopulation tend to make tissue more resistant to second dose of radiation; Reassortment and Reoxygenation tend to make it more sensitive. So, the overall sensitivity of the tissue depends on the fifth R, the Radiosensitivity defined as the relative susceptibility of cells, tissues, organs, organisms or other substances to the injurious action of radiation.

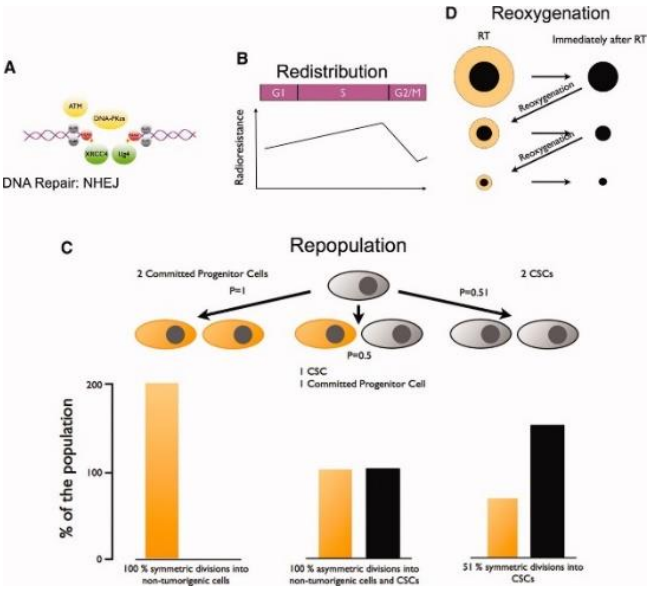

Figure 2.10: The 4 R of Radiobiology [27].

2.8 Radioprotection

Radioprotection is an autonomous discipline that arose as a field of application of radiobiology, to which it is linked. The aim of radiation protection is to protect humans and the environment from the harmful effects of radiation. It is based on the concepts of physics regarding the interactions of radiation with matter at the nuclear, atomic and molecular levels, of biology regarding the effects of these interactions at the cellular level, and of anatomic physiology about the consequences of these effects on tissues, organs, systems and the whole organism.

The system of protection against ionising radiation proposed by the ICRP (International Commission on Radiological Protection) is based on three principles:

- Principle of justification: according to which any activity with ionising radiation must be justified, i.e., the collective benefit obtained from the use of ionising radiation must outweigh the health detriment caused by its use.
- Optimisation principle: according to which exposure to ionising radiation should be kept as low as possible consistent with economic and social conditions.
- Principle of application of dose limits: in protectionism, a distinction is always made between reference levels for exposed workers and reference levels for the population. For the former, the legal limits are always higher than for the public,

to allow them to perform their functions in an environment where adequate field levels would not be possible. Without prejudice to the above principles of justification and optimisation, dose limits are set for workers and the public, which shall not be exceeded in the conduct of activities involving ionising radiation. This principle shall not apply to medical exposures.

Diagnostic Reference Levels are defined for patients, which are dose levels in medical radio-diagnostic practices or, in the case of diagnostic nuclear medicine, levels of radioactivity, for typical examinations for groups of patients of standard build and for types of equipment. These levels should not be exceeded for standard procedures, under conditions of correct and normal application about diagnostic and technical intervention.

2.8.1 Main formulas

The physical quantity used to quantify the interaction between radiation and matter is the absorbed dose. However, it has been observed that the biological effects of radiation depend not only on the absorbed dose, but also on the type of radiation and the tissue affected (tissues have different radio-resistance) by the radiation. For these reasons, the radiation protection quantities equivalent dose and effective dose were introduced.

Absorbed dose

The absorbed dose measures the amount of energy that radiation gives up to matter.

(2.17)

$$D = \frac{\Delta E}{m}$$

The unit of measurement in the I.S. (international system) is the gray (Gy), which is equivalent to the absorption of 1 joule (J) of energy per kilogram of matter.

Equivalent dose

The equivalent dose also considers the type of radiation and is given by the product of the absorbed dose (on a given organ or tissue) by a factor that depends on the type of radiation.

(2.18)

$$H = \sum_R w_R D_R$$

The unit of measurement in the I.S. (International System) is the sievert (Sv). In the case of X-rays, gamma or beta rays, 1 Gy of absorbed dose is equivalent to 1 Sv of equivalent dose.

Effective dose

The effective dose also considers the tissues that have been affected by the radiation and is defined as the summation over all organs of the equivalent dose for the individual organ by its tissue weighting factor.

(2.19)

$$E = \sum_{T} w_T H_T = E = \sum_{R,T} w_T w_T D_{T,R}$$

The effective dose is used to describe very briefly the effects of ionising radiation on individuals and the population. It is also measured in Sievert.

Isoeffect

A simplified way to find the equivalent effect (or isoeffect) of different fractionation regimens (dose/fraction and number of fractions; dose/fraction and total dose) of radiotherapy treatment, compared to the fractionation of an equivalent dose is obtained from the linear quadratic (LQ) model, not considering dose rate and total treatment time or corrections for repopulation occurring during the time interval of radiation treatment, in the form of the effective dose:

(2.20)

$$E = H\left(\alpha + \beta \frac{H}{N}\right) \qquad (H \leq 2\ Sv)$$

(2.21)

$$E = H \frac{\frac{\alpha}{\beta} + H}{\frac{\alpha}{\beta} + 2} \qquad (H > 2\ Sv)$$

In the formalism of the LQ model a ratio α/β = 3 is used for chronic effects and α/β = 10 for acute effects or tumour control action. For radiotherapy treatments without co-treatment, in summary:

(2.22)

$$n = n_0 e^{\alpha H + \beta \frac{H^2}{N}}$$

Where:

- n is the surviving cell population after irradiation;
- H is the total equivalent dose and N the number of fractions.

Some values used in modelling for α are between 0.75 and 0.075 and an α/β usually between 2 and (in the case of tumour tissues) 25 [28].

Chapter 3

3. FLASH Radiotherapy

3.1 FLASH Radiotherapy overview

In recent decades, the advent of radiotherapy (RT) has enabled the development of increasingly precise and powerful treatments for cancer patients. The main problem with RT is related to complications of irradiated healthy tissue, which therefore limits the dose to be used. Therefore, interest is now focusing again on a technique called FLASH radiotherapy. Indeed, preclinical studies in various animal models and a veterinary clinical trial have recently shown that, compared with conventional dose-rate radiotherapy, FLASH-RT could control tumours while minimising toxicity to normal tissues [29].

In contrast to conventional radiotherapy (CONV-RT), FLASH-RT provides a single high dose at an average dose rate of 40 Gy/s in milliseconds to achieve tumour control, while protecting normal tissues from damaging injury. It provides an intriguing prospect in improving clinical outcomes for cancer patients, as well as a new way to enhance differential responses between normal and tumour tissues. However, its mechanisms remain largely unclear.

The difference between FLASH-RT and CONV-RT is the duration of exposure to ionising radiation during the chemical stage. The effects initiated during the chemical phase by energy deposition during the physical phase depend strongly on the concentration of oxygen in the tissue. It can be assumed, given the role of oxygen in modulating radiosensitivity, that one of the mechanisms by which healthy tissues are less damaged than diseased tissues lies in the different oxygen concentration observed physiologically between the two types of tissue. In fact, there is no change in radiosensitivity at tumour level. The delivery of the dose in an extremely short time (ultra-high rates) would cause a rapid consumption of local oxygen (oxygen depletion effect). The rapid depletion of oxygen would then cause radiation-induced hypoxia of a transient nature, which would result in increased radio-resistance of healthy tissues, but would not

affect tumours, which are already partially hypoxic. The net result would therefore be an increase in the so-called therapeutic window, a fundamental concept in radiotherapy.

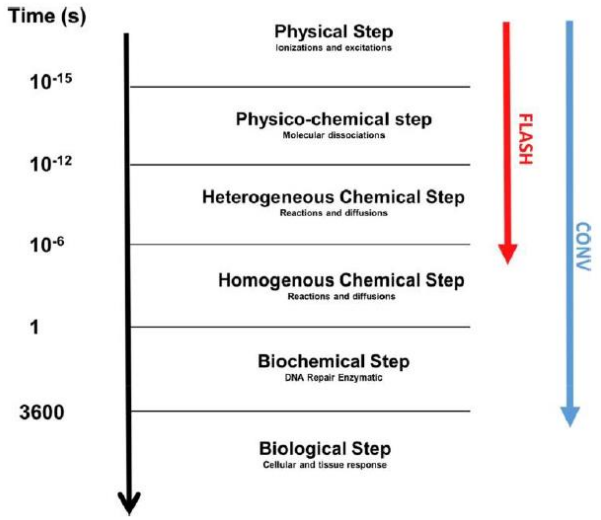

Figure 3.3: Comparison between FLASH-RT and CONV-RT [29].

As already mentioned, FLASH-RT involves the ultra-rapid delivery of RT at doses generally several thousand times higher than those currently used in CONV-RT. The full definition is more complex and involves several interdependent physical parameters such as repetition rate, pulses (number and width), and total exposure duration. The first obvious difference between FLASH-RT and CONV-RT is the time required to deliver the dose, which varied from microseconds to hundreds of milliseconds for FLASH-RT but increased to minutes for CONV-RT. This extremely short exposure time made possible by FLASH-RT suggests an early modulation of radiochemical events that depend on the concentration of oxygen in the irradiated volume. FLASH-RT could cause rapid local oxygen consumption and result in transient radiation-induced hypoxia.

Another major challenge is to translate FLASH-RT into the clinic because the aim is to develop optimal technology in terms of high-precision delivery similar to the technology currently used for CONV-RT. Indeed, the biological sparing of normal tissue offered by FLASH-RT should be seen as complementary to the powerful normal tissue sparing effect offered by high precision delivery but could not and should not replace it. The potential risks associated with ultra-rapid administration of FLASH-RT should be considered prior to its clinical use. FLASH-RT involves the delivery of a limited number of pulses ($\leq$10 pulses). Safe delivery can be achieved by using a dose monitoring and stopping system, capable of monitoring the dose pulse by pulse. The required high-speed detectors, fast

signal acquisition and electronic processing technologies are routinely used in high-energy physics laboratories to control large particle accelerators and are adaptable to FLASH-RT systems [29].

3.2 Flash effect

An important warning of pre-clinical studies investigating FLASH-RT is the lack of consistency between variables that could potentially influence the induction of the FLASH effect such as: dose rate, total dose, pulse rate, fractionation and radiation mode. The dose rate required for a FLASH sparing effect might not be universal but rather tissue-specific, model- and/or assay-specific, or there might be dosimetrical differences between the two delivery modes/settings, which highlights the challenge in conducting studies at these dose rates, finding and exploring a beneficial FLASH effect [30].

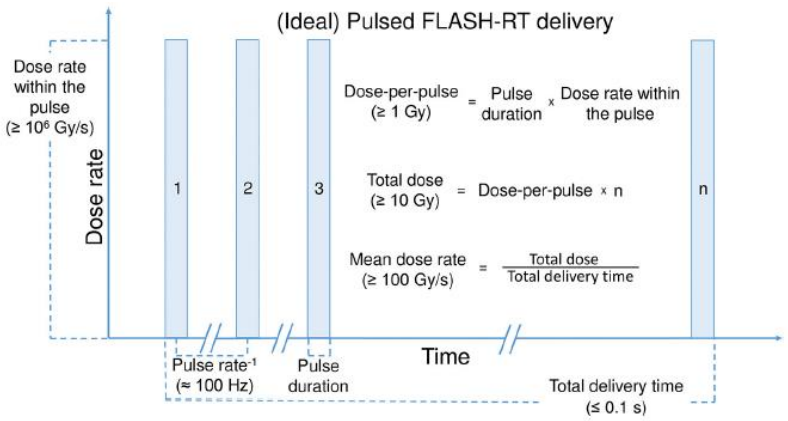

Figure 3.2: Ideal Pulsed FLASH-RT delivery [30].

However, two concepts can be defined to give a better understanding of what the flash effect is:

- Normal Tissue Sparing: the FLASH effect is defined as the decrease in radiation-induced normal tissue toxicities with dose delivery at ultra-high dose rates (FLASH), compared to conventional dose rates used clinically.
- Tumor Control: an important attribute of FLASH that has been reported in only a limited number of studies, is the ability to generate a similar anti-tumor response as the equivalent conventional dose-rate radiation. This potentially means that larger doses could be administered to radioresistant tumors using FLASH radiotherapy due to the increased therapeutic index [31].

3.3 Hypotheses to explain FLASH effect

With the improvements in modern-day technology and a greater understanding of radiobiology, FLASH is demonstrating potential as a key tool in the future of clinical radiotherapy. Before this can happen though, it is critical that the underlying biological mechanisms and optimal beam delivery parameters are realized, as these currently remain largely uncovered. The following are the most widely accepted hypotheses to explain the mechanisms underlying FLASH-RT.

3.3.1 Oxygen Depletion

The biological mechanism responsible for the reduction in normal tissue toxicities following irradiation at FLASH dose rates is not currently understood, yet several non-mutually exclusive hypotheses have been proposed. Some researchers have suggested that the differential response between FLASH-RT and CONVRT may be due to the radiochemical depletion of oxygen at ultra-high dose rates and subsequent radio-resistance conferred to the irradiated tissue. It is widely accepted that hypoxic tissues are more radioresistant than well-oxygenated tissues. This is because in the presence of molecular oxygen there is fixation of indirect radiation-induced DNA damage. Indirect damage, the predominant mechanism by which low linear energy transfer (LET) radiation induces DNA damage, occurs when radiation results in the radiolysis of water molecules and the subsequent generation of hydroxyl radicals. Hydroxyl radicals are then incorporated into DNA, causing damage, yet this can be easily resolved. However, if a hydroxyl radical reacts with molecular oxygen, this yields a peroxyl radical. Peroxyl radicals have the potential to induce permanent damage and are therefore a more efficacious DNA damaging agent. Hence, a lack of oxygen in the immediate environment of a cell limits the extent of radiation-induced DNA damage. Together, these data suggest that the irradiation of tissues with FLASH-RT results in radiochemical oxygen depletion, giving rise to an extremely acute period of hypoxia within the irradiated tissue and consequently a transient radio-resistance. This phenomenon is not seen following irradiation with CONVRT as radiation is delivered with much smaller pulses and over a longer timeframe. Hence during CONV-RT, oxygen depletion is limited, and there is sufficient time for oxygen to diffuse into the irradiated region to replace oxygen that has been lost. Therefore, oxygen concentration within the irradiated tissue is maintained. There is growing interest surrounding other oxygen-based radicals as a potential

mechanism bridging the local oxygen depletion observed following irradiation at ultra-high dose rates, and reduced toxicities to normal tissue. A recent study proposes that oxygen depletion at ultra-high dose rates promotes the protection of normal tissue by limiting the production of reactive oxygen species (ROS). The oxygen depletion hypothesis seems to explain the reduced toxicity of FLASH-RT to normal tissue. However, it does not easily explain how FLASH-RT can maintain tumor response relative to CONV-RT. Although tumors are more hypoxic compared to their normal tissue counterparts, most are not completely anoxic. Therefore, following the use of FLASH-RT, there will also be radiochemical oxygen depletion within the tumour, so this would be expected to confer radio-resistance to the tumour [30].

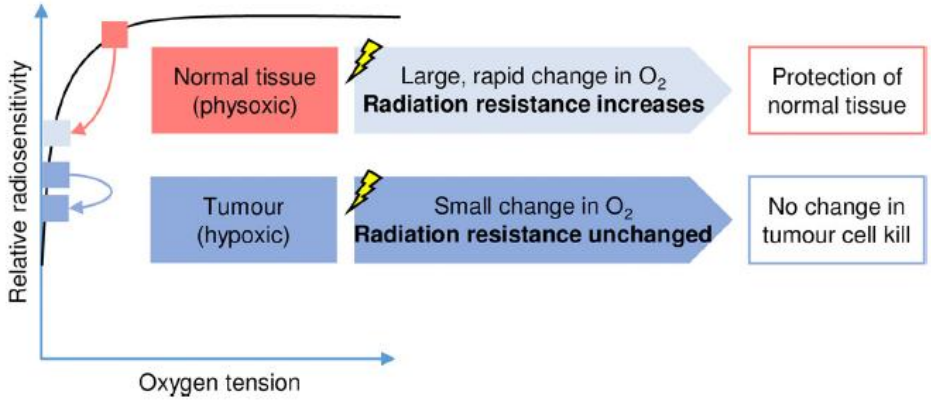

Figure 3.3: The oxygen depletion hypothesis [30].

3.3.2 Immune Response

A modified immune response following FLASH-RT relative to CONV-RT has also been proposed as a potential mechanism for the FLASH effect. The fractionated RT regimes commonly used in CONV-RT, result in the irradiation of a greater proportion of circulating lymphocytes compared to total dose delivered in a single fraction. Additionally, it has been reported that the induction of chromosomal aberrations in the circulating blood pool is dependent on the total volume of the blood pool irradiated. Therefore, in accordance with the short irradiation time, characteristic of FLASH-RT, it would follow that fewer lymphocytes would be irradiated and subsequently reduced induction of chromosomal aberrations. However, FLASH-RT would expose lymphocytes to a greater dose of radiation, albeit much fewer of them, in comparison to CONV-RT. If a modified immune response contributes to the FLASH effect, one expects a fractionated FLASH-RT regime to, at least in part, reduce any protection conferred by the FLASH effect. It is worth noting however, that any evidence linking an immune role to the

FLASH effect is correlative rather than causative; it is unclear whether any differential immune response following irradiation at ultra-high dose rates contributes to the FLASH effect or is a consequence of it. Additionally, since the FLASH effect has been observed in vitro in bacterial and cell culture models, which are devoid of a functioning immune system, any immunological component is likely to be responsible for only part of the underlying mechanism. More studies are needed to clarify if the immune response or other biological responses like DNA damage response or inflammation is different following FLASH-RT compared to CONV-RT, and if they are part of the underlying mechanism resulting in the FLASH effect [30].

3.3.3 DNA damage

Classic Target Theory considers DNA as the major target of ionizing radiation. DNA damage, especially unrepaired DNA double strand breaks, is a key factor determining the cellular response. The faster and more precise recovery of normal tissues from radiation-induced DNA damages, compared to tumors, is the basis of routine hyperfractionation radiotherapy. How much difference is caused by FLASH-RT between normal cells and tumor cells in DSB yields and the precision in DSB repair has not yet been quantified. However, there are likely to be intrinsic differences between normal tissues and tumor tissues in response to DNA damage response [32].

3.3.4 Other possibilities

Experimental data indicating FLASH effects consistently include the sparing of stem cells including epidermal, neural, and intestinal stem cells. It is suggested that the FLASH effects are probably due to specific sparing of hypoxic stem cell niches so that the oxygen depletion spares these normal stem cells. As such, FLASH-RT theoretically should spare tumor stem cells as well because tumor stem cells possess hypoxic stem cell niches. Conceptually, FLASH-RT spares both normal and tumor stem cells cannot provide a reasonable explanation for that FLASH-RT inhibits tumor growth but spares normal tissue. There are proofs that tumor stem cells are radioresistant to CONV-RT but there are no experimental data on the effects of FLASH-RT on tumor stem cells yet. Comparable studies on the effects, specifically DNA damage response and its related immunoreaction, of FLASH-RT on normal and tumor stem cells are called upon to provide considerable clues [32].

3.4 Different types of FLASH-RT

Another question that needs to be answered is which radiation source is best to provide FLASH radiotherapy. Much of the current evidence has used electron sources, however this is currently limited to the treatment of superficial tumours or intraoperative radiotherapy. Proton FLASH-RT may offer the best solution to be able to treat some deep tumours. However, the implementation of proton FLASH-RT still has its technical limitations, as to deliver protons to a large tumour volume, the proton beam must be dispersed, which may cause particle loss and decrease the total dose delivered. In addition, research using protons has produced largely conflicting results, and it is also still unknown how increasing the LET at and around the Bragg peak will impact the FLASH effect. Therefore, much more research on proton FLASH-RT, particularly investigations at physiological oxygen concentrations, is needed for this to potentially be translated into the clinic for the benefit of cancer patients.

Alternatively, the development of FLASH-VHEE or FLASH-X-ray devices is needed to treat tumours located deep in patients.

Building a clinical device capable of delivering x-rays FLASH-RT beams involves solving significant technical challenges. These include that the power of the accelerator should be at least 100 times higher than that used to produce FLASH electrons and that the conversion lens to generate photons should have specific characteristics to withstand enormous instantaneous power. As far as FLASH-RT using VHEEs (very high-energy electrons) is concerned, it is currently confined to pure experimental research, since these particles are only produced with experimental plasma accelerators (150-250 MeV).

Considering that with the use of photons and electrons the sparing of healthy tissue increases with the use of radiotherapy FLASH, with protons then the flash effect should increase even more as these particles are favoured by the inverse dose profile of the Bragg curve. Furthermore, protons, by their very nature, are ballistically more precise and release the dose while sparing much more healthy tissue than conventional RT. The proton beam loses energy because it is progressively slowed down to the point where the particles stop. At this point, called the Bragg peak, all residual particle energy is released, and the damage done to the target tissue is maximised.

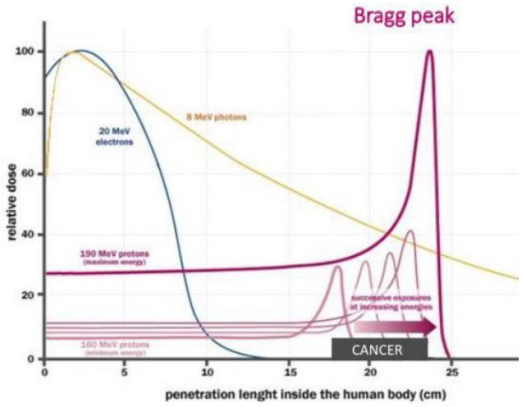

Figure 3.4: Bragg's peak [33].

The most promising types of FLASH-RT are analysed below.

VHEE FLASH-RT

Very High Energy Electrons (VHEEs) provide more favourable dose distributions than conventional radiotherapy electron and photon beams. Plane-parallel ionisation chambers are the recommended secondary standard systems for clinical reference dosimetry of electrons, therefore chamber response to these high energy and high dose-per-pulse beams must be well understood. Want to be used because a low energy of the electron beam generates a major obstacle in their translation to future clinical trials of FLASH due to limited penetration depth. The application of Very High Energy Electrons (VHEEs) in radiotherapy, with energies up-to 250 MeV, could overcome this depth limitation due to significantly increased practical range and improved penumbra for deep-seated tumours with respect to currently available clinical photon beams, which (in contrast to VHEE) cannot be delivered in a regime which induces the FLASH effect. Moreover, VHEE beams can provide more conformal dose distributions to deep seated tumours, in comparison to current advanced electron radiotherapy techniques, whilst reducing the integral dose and organ-at-risk dose. There is also the possibility of focusing VHEE beams into the patient, reducing peak surface and exit doses for a single beam by more than one order of magnitude compared with a collimated beam. Moreover, VHEE radiotherapy would benefit from reduced scattering and divergence, leading to a reduction in healthy tissue irradiation surrounding the tumour [33].

Proton FLASH-RT

Proton therapy implants operating with pencil beam scanning (PBS) can produce very high instantaneous dose-rates in the order of 200 Gy/s. However, the duration of the

scanning process lowers the current average dose-rate (1-2 Gy/min) which limits investigations of the FLASH effect with protons over large irradiation fields. In fact, dose rates of 5 Gy/s are already considered as ultra-high dose rates in this field. FLASH proton therapy does not seem to influence acute effects, as no significant difference in overall cell survival was observed between low and high dose rates at a dose of 10 Gy. However, an influence on late adverse effects was observed. This long-term beneficial effect could be due to the high proton dose rate influencing the long-term balance between anti and pro-inflammatory molecules. The different small-scale energy distribution of protons compared to electrons could be a reason for the lack of beneficial response to FLASH irradiation [34].

Developing accelerator technology to meet the requirements for FLASH proton delivery is challenging. Whilst experiments have already been carried out with protons at FLASH dose rates, these have been limited so far to small volumes. Significant development will be required to enable FLASH delivery beyond these limitations, particularly if the goal is to adapt existing spot-scanning systems for use at FLASH dose rates to clinically relevant volumes. Developments in magnet scanning speed and dosimetry will be necessary before such systems can be realised. The hybrid approaches already being pursued, particularly the use of scanned beams with patient-specific range modulators, are likely to pave the way to clinical proton FLASH delivery. Each accelerator type has its own challenges to meet this goal [35].

Carbon ions FLASH-RT

Although the exact mechanisms underlying FLASH are still unclear, it has been suggested that radiation delivered at high dose rates spares normal tissue via oxygen depletion. In addition, heavy-ion radiation achieves tumor control with reduced normal tissue toxicity due to its favourable physical depth-dose profile and increased radiobiological effectiveness in the Bragg peak region. Studies have shown that very high-dose carbon ions generate more and more molecular oxygen towards the end of their trajectory at the Bragg peak, which is located within the tumour in clinical radiotherapy with heavy ions. This finding indicates an increase in cell-killing potential by carbon ions. These early results suggest that with the use of FLASH-RT with energetic carbon ions, an even better therapeutic ratio can be achieved due to the creation of an oxygenated

environment in the tumour, which contributes to increased cell killing efficacy while simultaneously protecting normal tissue [33].

3.5 Clinical perspectives for FLASH therapy

The obvious endpoint of investigation into the FLASH effect is the translation of FLASH-RT to the clinic. FLASH-RT could be translated to the clinic to serve two general purposes:

- Firstly, the FLASH effect could be exploited to allow for escalation of total dose in the treatment of radioresistant tumors that are currently associated with poorer patient outcomes. In this case, it is hypothesized that a greater dose of radiation could be delivered to the tumor without inducing as severe toxicities to the normal surrounding tissue as would be expected following CONV-RT.
- Secondly, FLASH-RT could be used in situations in which RT confers good levels of tumor control but is associated with severe normal tissue toxicity—the same total dose would be administered, but hypothetically FLASH-RT would induce less severe toxicities compared to CONV-RT [30].

Studies to date have shown that FLASH-RT is consistently associated with relative sparing of normal tissue:

- In various tissue types;
- In different animal species;
- With various types of beam and energy.

But there are no tumour-sparing effects with FLASH-RT. The experimental conditions for observing a FLASH effect were essentially:

- Small volumes of normal tissue (a few cc);
- Mainly single dose (> 7-10 Gy);
- Total treatment time < 100-200 ms.

These are three limitations for the clinical translation of RT. For example, at the moment it is not known the effect in large volumes of normal tissue. Second aspect regarding the use of fractionation with flash and also, it need to explore more the interaction between fractionation and flash. Third point is how will be able to modulate the dose in such short

time scale. The other issue for clinical translation is what about the magnitude of the flash sparing effect on normal tissues. We know that it is probably variable, it may be generally between 20% and 35% of the dose that appears to be spared and it may be different from each type of tissues and organ at risk.

Clinical translation is ongoing now, an example is the use of electrons in patients with skin cancer [36].

Chapter 4

4. Radiobiological models

Compared to conventionally used therapies, the advantage of radiotherapy is to irradiate in a more targeted manner the tumor cells than the healthy cells surrounding the tumor. The goal, therefore, is to optimize the so-called therapeutic ratio (the ratio that evaluates the probability of eliminating the tumor with respect to possible complications of healthy tissues). In this context, *radiobiological models* are introduced. A radiobiological model of cellular inactivation is defined as a mathematical formulation that models the essential characteristics of the cellular structure and of the irradiation process with the aim of deriving the radiobiological parameters that define the radiosensitivity of tissues as a function of the irradiation conditions. The purpose of these models is to provide TPSs with the tools to evaluate the biological effect associated with the dose distributions calculated in the planning phase. Among these parameters, belonging to the branch of dosimetry, the most relevant for modelling purposes is the RBE, already discussed in Chapter 2 (equation 2.3).

4.1 Microdosimetric quantities

Energy exchange between matter and radiation occurs through discrete interactions distributed both along the particle track and between tracks. To understand the mechanisms of action of radiation at the cellular and sub-cellular level, conventional dosimetry is not sufficient, since radiation fields that might appear uniform at the tissue or cell level, can be completely inhomogeneous at the sub-cellular level. Therefore, such phenomena are studied by microdosimetry, a science that studies the microscopic properties of ionizing radiation interactions and the geometric distribution of various energy depositions, considering their inhomogeneity and the stochastic nature of the interactions [39]. Two quantities of fundamental importance in microdosimetry are: the specific energy and the lineal energy.

Specific energy

The energy imparted ε to a given site is a random variable that takes on a well-defined value in a fixed region at the end of an irradiation, but that, in repeated irradiations, takes

on different values that are distributed according to certain probability functions. The fluctuations of the values that it assumes are the greater the smaller the site, the smaller the dose and the more densely ionizing is the radiation in question.

Dividing the imparted energy by the mass of the site yields the specific energy z, i.e.:

(4.1)

$$z = \frac{\varepsilon}{m}$$

Lineal energy

Through ε_1, the energy imparted in single events, we can define a new quantity, the lineal energy y as:

(4.2)

$$y = \frac{\varepsilon_1}{l}$$

where l indicates the mean chord and represents the characteristic length of the site and is l=4V/S, V and S being the volume and surface area of the site.

The lineal energy represents the microdosimetric analogue of the LET. Probability distributions can be defined for both quantities [39].

RBE

One way to calculate the effectiveness of a radiation compared to the reference radiation, conventionally associated with x-rays, is Relative Biological Effectiveness. In the case of Hadrontherapy, for example, the RBE of protons is assumed to be a constant value of 1.1, however, it is known that this quantity cannot be assumed as a constant, since it depends on both physical and biological factors. It is necessary to know the trend of RBE as a function of quantities such as LET, dose, tumor depth and to see how it changes with tissue type [37].

Since the RBE depends on several factors, it is possible that two types of uncertainties emerge in determining its value. These are called *range straggling* and *biological range extension*. The first one is due to the particles straggling by the matter: it is a stochastic event because there is no certainty that all particles stop at the same depth and at the same energy value. The consequence is that the Bragg peak does not coincide perfectly with the assumed one. The second is due to the dependence of the RBE on dose, LET, and α/β

ratio. The RBE varies as these parameters change and this could cause an abrupt increase in the distal part of the SOBP, where healthy tissues reside [38].

4.2 LQ-based models

Radiobiological models are divided into LQ based and non-LQ based.

Regarding the former, these are based on the linear quadratic model of cell survival curves, which is mainly used through the α and β parameters. Using the LQ model, it is possible to calculate the fraction S of cells that survive irradiation as follows:

(4.3)

$$S = e^{-\alpha D - \beta D^2}$$

From which it is possible to calculate the RBE, remembering that it causes, for any irradiating particle used, the same effect as an x-ray beam:

(4.4)

$$\alpha_x D_x + \beta_x {D^2}_x = \alpha_p D_p + \beta_p {D^2}_p$$

(4.5)

$$RBE\left(D_p, \alpha_x, \beta_x, \alpha_p, \beta_p\right) = \frac{\sqrt{{\alpha^2}_x + 4\beta_x D_p\left(\alpha_p + \beta_p D_p\right)} - \alpha_x}{2\beta_x D_p}$$

The main LQ-based models are those of Wilkens and Oelfke, Wedenberg and Carabe-Fernandez, in which equations 4.3, 4.4 and 4.5 are taken as the basis for deriving an analytical expression of the RBE, with different dependencies of the radiosensitivity parameters on LET and dose.

Wilkens-Oelfke model

In this model we assume a trend of the α_p parameter increasing with LET and dependent on a λ parameter. It is worth mentioning that this model is only valid for radiation with LET up to 30 KeV/μm. Then, α is parameterized as a function of LET L, as:

(4.6)

$$\alpha(L) = \alpha_0 + \lambda L$$

With α_0 free parameter. Instead, β_p is constant and equivalent to that of the reference radiation:

(4.7)

$$\beta_p \coloneqq \beta_x$$

At this point, the predicted RBE trend can be derived:

(4.8)

$$RBE\left(D_p, L, \alpha_0, \lambda, \alpha_x, \beta_x\right) = \frac{\sqrt{\alpha^2{}_x + 4\beta_x D_p\left(\alpha_0 + \lambda L + \beta_x D_p\right)} - \alpha_x}{2\beta_x D_p}$$

RBE predicted by this model increases as LET increases [40].

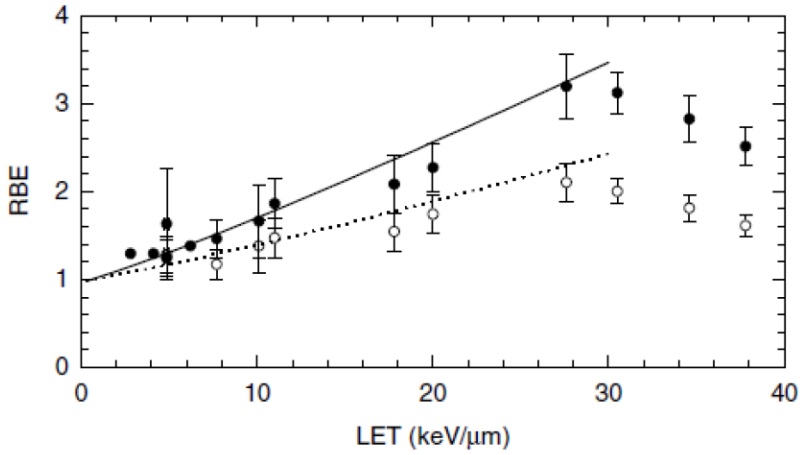

Figure 4.1: RBE of protons as a function of LET with the Wilkens-Oelfke model [40].

Wedenberg model

In this case, instead of the simple α_x parameter, the ratio (α_p/α_x) is considered, but the dependence on the LET is still linear:

(4.9)

$$\frac{\alpha_p}{\alpha_x} = 1 + kL$$

The difference with the previous model is that the slope of the line cannot be a free parameter but, must depend on the type of tissue in which one is located [41]. This dependence enters the equation of (α_p/α_x) through the tissue response parameter $(\alpha_p/\alpha_x)_x$:

(4.10)

$$\frac{\alpha_p}{\alpha_x} = 1 + \frac{qL}{(\alpha/\beta)_x}$$

Again, assuming $\beta_p = \beta_x$ we derive RBE:

(4.11)

$$RBE\left(D_p, L, \left(\frac{\alpha}{\beta}\right)_x\right) = -\frac{1}{2D_p}\left(\frac{\alpha}{\beta}\right)_x + \frac{1}{D_p}\sqrt{\frac{1}{4}\left(\frac{\alpha}{\beta}\right)_x^{\ 2} + \left(qL + \left(\frac{\alpha}{\beta}\right)_x\right)D_p + D^2{}_p}$$

This expression is valid only in cases where the LET is less than 30 KeV/µm. Higher LETs, however, are not very relevant in the context of cancer treatment, so the equation has almost general validity. Looking at the figure 4.2, one can see the different variables that affect RBE: it increases as dose and $(\alpha/\beta)_x$ decrease and as LET increases, but this is only valid for tissues with low $(\alpha/\beta)_x$ [41].

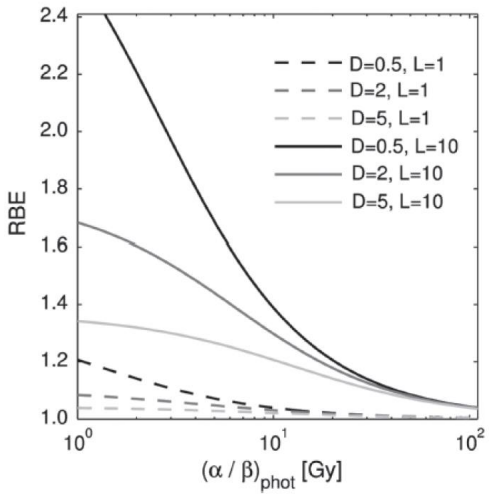

Figure 4.2: RBE predicted by the Wedenberg model as a function of $(\alpha/\beta)_x$ [42].

Carabe's model

This model considers, like the previous ones, the dependence of RBE on parameters such as dose, LET and the value of α and β, but assumes that the β parameter may depend on LET, while in previous cases it was always assumed to be constant. In this model, two quantities are identified: RBE_{max}, defined as the ratio of the slopes of the zero-dose survival curve for the radiation under investigation and the reference radiation, respectively, and RBE_{min}, defined as the root of the ratio of the beta parameters of the

radiation at high and low LET, respectively, assuming precisely that this parameter depends on the LET [42].

(4.12)

$$RBE_{max} = \frac{\alpha}{\alpha_x}$$

(4.13)

$$RBE_{min} = \sqrt{\frac{\beta_H}{\beta_L}}$$

At this point it is possible to calculate the RBE. Note that this depends entirely on parameters related to the radiation at low LET and that it is inversely proportional to the dose, since when it tends to 0 the equation of RBE tends to RBE_{max}, while when the dose tends to infinity the equation reduces to that of RBE_{min}.

(4.14)

$$RBE = \frac{\left(\frac{\alpha}{\beta}\right)_x RBE_{max} + \sqrt{\left(\frac{\alpha}{\beta}\right)_x^{\,2} RBE_{max}^{\,2} + 4D_x RBE_{min}^{\,2}\left(\left(\frac{\alpha}{\beta}\right)_x + D_x\right)}}{2\left(\left(\frac{\alpha}{\beta}\right)_x + D_x\right)}$$

4.3 Non LQ-based models

Cell survival depends not only on dose, but also on ion species and ion energy. Consequently, particularly in the context of hadrontherapy, more complex models than those described above are needed to predict the biological effect of radiation to perform rigorous treatment planning. However, due to the complexity of radiochemical and radiobiological mechanisms involved in the formation of biological damage, the development of such models is very complex. To date, there are several models of cellular inactivation, each developed by different research centres. The main ones are:

- LEM (Local Effect Model);
- MKM (Microdosimetric Kinetic Model);
- RMF (Repair Misrepair Fixation).

4.3.1 Local Effect Model LEM

LEM was developed in Germany at GSI (Gesellschaftfur Schwerionenforschung) and is currently used in the planning of many treatments, not only with protons but also with heavy ions. According to this model, the damage caused by irradiation depends only on the dose deposition in the tissue and not on the type of radiation used. Over time, the model has been modified and improved several times and today the LEM IV version is used in which the biological damage is determined more precisely by the disruption of the DNA double helix [43].

To cope with the needs of a precise determination of RBE for therapy, LEM has been developed as a continuation of the models based on track structure. LEM also uses three basic inputs: the radial dose distribution inside the particle tracks, the average size of the biological target, i.e., the cell nucleus, and the respective dose-response curve for sparsely ionizing radiation as usually measured in x-ray experiments. In a Monte Carlo calculation, tracks are overlaid on the critical target, which is assumed to have no internal structure, i.e., a homogeneous distribution of the sensitive sites inside the nucleus [44].

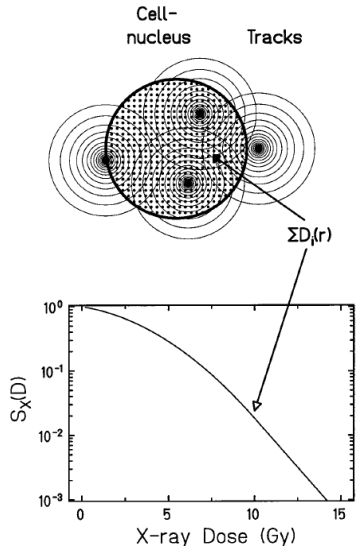

Figure 4.3: Principle of the local effect model [44].

This target is then divided into cylindrical zones according to the radial dose distribution in such a way that the dose in each zone is constant within a few percent. For these zones, the probability of the induction of a lethal lesion is calculated according to the x-ray dose-effect curves. For each dose, the measured inactivation is assumed to correlate to the number of lethal lesions by a Poisson distribution. Therefore, the probability of a lethal

lesion in a nucleus of volume V is calculated as the logarithm of survival S normalized to the volume V, and the density of lethal events is given by:

(4.15)

$$\frac{ln\, S(D)}{V}$$

Integration over the complete volume of the cell nucleus finally yields the total expectation value for the induction of lethal events:

(4.16)

$$N = \int \frac{ln\, S(D)}{V} dV$$

And the survival is:

(4.17)

$$S = e^{-N}$$

In this equation, dV describes the volume elements that are dissections of the radial dose with the cell nucleus. The dose dependence enters via the x-ray dose effect curve S(D). Because the local dose in a particle track expands to mega-Gy, where no experimental data exist, the usual dose-effect curve in a linear quadratic form is extrapolated to these extremely high doses by an exponential function that fits the slope for the highest doses measured. Thus, the survival curve is described by these parameters: the α, β at low doses, and the threshold dose for the transition of linear quadratic to exponential slope. However, the choice of these parameters is not essential to the model; in principle, it yields the same results if the data of a measured survival curve are used according to their numerical values.

Because the important transition between repair and non-repair occurs at doses where the dose-effect curve is described by a and b terms, the calculated RBE strongly depends on the α/β ratio in this model. A large α/β ratio, i.e., an approximation to a pure exponential shape, yields a small or no RBE maximum, while small a-b ratios yield large RBE values. These calculations confirm the experimental findings and produce an elevated RBE for biological systems with shouldered survival curves. The saturation effect at high particle doses yields the observed decrease in RBE (overkill effect) [44].

4.3.2 Microdosimetric Kinetic Model MKM

This model was developed by Hawkins in 1994 and then modified over the years. The model is based on a microdosimetric approach in which cell nuclei are divided into volumes, called domains, of 1 μm within which the RBE varies as the energy released by the charged particles varies.

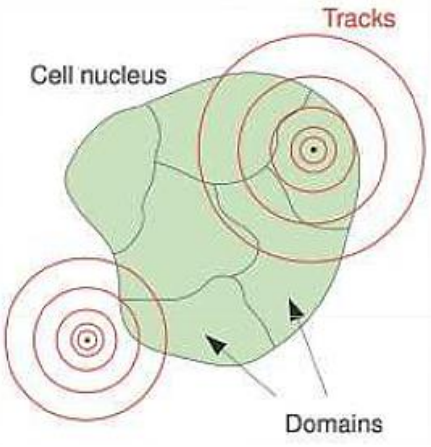

Figure 4.4: Microdosimetric approach in MKM model [45].

In domains, energy can cause two types of damage, lethal and sublethal damage, on which cell death or survival depends. Currently, a modified version of the MKM, devised by Kase, is used that considers overkill effects and in which the cell survival curve is given by the following formula [45]:

(4.18)

$$S = \exp\left[-\left(\alpha_0 + \frac{\beta}{\rho\pi r^2{}_d} y^*\right) D - \beta D^2\right]$$

Where:

- D is absorbed dose;
- α_0 is a parameter which depends on the survival curves for x-rays and charged particles, and taken as a constant;
- r_d is the radius of the domain and ρ its density;
- y^* is the average energy in dose, corrected for saturation. It can be calculated as:

(4.19)

$$y^* = \frac{{y^2}_0 \int \left(1 - \exp\left(-\frac{y^2}{{y^2}_0}\right)\right) f(y)dy}{\int y f(y)dy}$$

Here, f(y) is the probability density of the energy, y is called lineal energy and is the ratio between the energy absorbed in the ionization event and the average chord length of the domain and y_0, finally, is a saturation parameter.

Considering the survival curve, the RBE can be calculated:

(4.20)

$$RBE = \frac{2\beta D}{\sqrt{{\alpha^2}_x - 4\beta \ln(S)} - \alpha_x}$$

Figure 4.5 shows that the biological effectiveness calculated with this model increases with depth, reaching a maximum along the SOBP and then decreasing again. In addition, he maximum value of RBE depends on the initial energy of the particle beam and that it decreases as the energy increases [45].

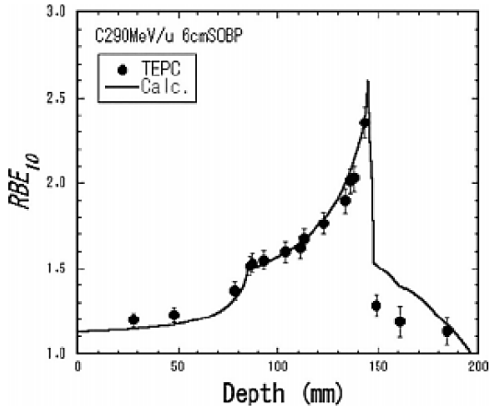

Figure 4.5: RBE distribution [45].

4.3.3 Repair Misrepair Fixation RMF

The RMF was developed by Carlson et al. in 2008. This model is developed to better link double-strand break (DSB) induction to reproductive cell death. Formulas linking linear quadratic (LQ) model radiosensitivity parameters to DSB induction and repair explicitly account for the contribution to cell killing of unregainable DSBs, misrepaired and fixed DSBs, and exchanges formed through intra- and intertrack DSB interactions. Information

from Monte Carlo simulations is used to determine the initial yields and complexity of DSBs formed by low- and high-LET radiations [46].

For a single dose of radiation delivered over a short time interval, the LQ model is commonly used to relate absorbed dose D, to biological effect ε, through two radiosensitivity parameters (α and β). In general, α and β depend on many factors, including the nature of the irradiated tissue, oxygen concentration, and radiation type and quality. In the RMF model, reproductive cell death by mitotic catastrophe, apoptosis, or other cell death modes is explicitly linked to DSB induction and processing. This model has shown that the effects of radiation quality, q, on α and β for particles with a stopping power up to at least 100 to 150 keV/mm can be modelled using:

(4.21)

$$\alpha(q) = \theta \sum(q) + \kappa \overline{Z_F}(q) \sum(q)^2$$

(4.22)

$$\beta(q) = \left(\frac{\kappa}{2}\right) \sum(q)$$

Here, ∑ is the initial number of DSB per Gray per giga base pair (Gy^{-1} Gbp^{-1}), $\overline{Z_F}$ is the frequency-mean specific energy (Gy), and q and κ are tumor or tissue-specific parameters related to the biological processing of initial DSB.

RBE is defined as the ratio of a low-LET reference dose to a dose with radiation quality q that produces the same biological effect:

(4.23)

$$RBE = \frac{\sqrt{\alpha^2{}_x + 4\beta_x D(\alpha_D + \beta_D D)} - \alpha_x}{2\beta_x D}$$

Substituting the equations 4.21 and 4.22 in 4.23 results in:

(4.24)

$$RBE = \frac{1}{2D}\left[\sqrt{\left[\left(\frac{\alpha}{\beta}\right)_x + 2D\frac{\sum_D}{\sum_x}\right]^2 + \frac{8D}{\sum x^2}\left((\overline{Z_F}\,\Sigma^2)_D - \overline{Z_{F,X}} \sum x \sum D\right)} - \left(\frac{\alpha}{\beta}\right)_x\right]$$

Within this model, RBE depends on $\left(\frac{\alpha}{\beta}\right)_x$ but is independent of α_x [47].

4.4 Models comparison

Having analysed the main radiobiological models, it is possible to compare them by analysing the trend that is predicted for the RBE based on experimental data.

4.4.1 LQ-based models comparison

The figure 4.6 shows that, in general, all models show a stable RBE value in the area before SOBP, a steep increase in the distal area and a more constant increase in the central area. The Wedenberg model comes closest to the experimental results. The Wilkens-Oelfke and Carabe models show a higher RBE value, but close to the standard deviation of the experimental one [48].

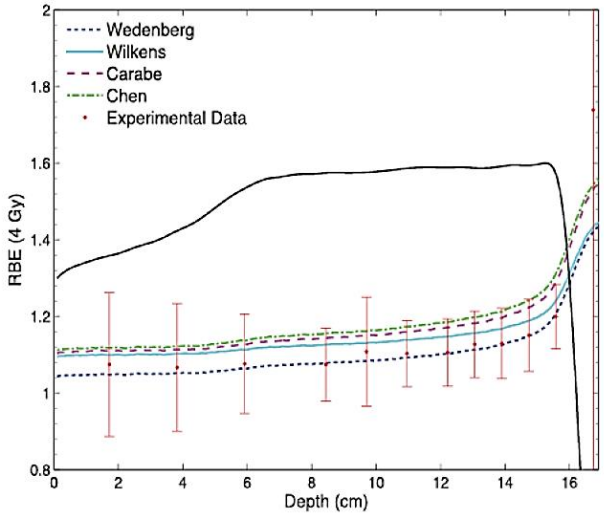

Figure 4.6: RBE values predicted by LQ-based models [48].

4.4.2 Non LQ-based models comparison

In this case the main comparison is between LEM and MKM because they have similarities:

- the principal target is the cell nucleus for any radiation quality;
- the nucleus is divided into small independent sub-volumes;
- a cell survival curve for x-rays is adopted as the local dose-effect curve of each sub-volume;
- the summation of the local effect in all sub-volumes over the whole nucleus determines the cell survival probability.

The size of the sub-volumes and the dose-effect curves are different between the MKM and LEM. In principle, the MKM focuses on the stochastic energy deposition in a micron-size domain while the LEM considers the local dose of infinitesimally small regions. Therefore, in MKM, the cell survival curve can be simulated from the experimentally obtained specific energy spectra obtained by a microdosimetric approach while the LEM uses a theoretical amorphous track structure model [49].

The most significant difference between MKM and LEM is related to the definition of the input parameters. In LEM, all parameters are, at least in principle, defined by measurable quantities, whereas in MKM, domain size, a critical parameter, is currently not a measurable quantity, as it cannot be uniquely identified with any known structure in the cell or cell nucleus. Furthermore, in LEM model the β parameter is dependent on LET and particle type, whereas in the MKM the photon-related dose-effect relationship is parameterised by the linear quadratic model whatever the dose range and the β parameter is independent of LET and particle type.

Both models use the same approximation of the correction for high-LET particles caused by a non-Poissonian distribution of lethal events. This correction requires the nuclear size to be the target size to determine the impact statistic. However, the method used to determine the nuclear radius differs between the two models. In the LEM the effective nuclear radius is calculated from measurements of the nuclear zone distribution, in the MKM the radius is assumed from the fit of the experimental results regardless of the size distribution. It can be concluded that the differences between the two models depend on the different methods used to calculate the biological effect of a dose.

Figure 4.7 shows the predictions of the RMF model, the MKM, the amorphous track based MKM and the track structure model. All models predict a relatively stable value for the RBE proximal to the SOBP and a steep increase beginning in the distal part of the SOBP. Except for the amorphous track based MKM, there is a modest increase in RBE throughout the proximal and central plateau of the SOBP. In the final analysis, the models by Wilkens and Oelfke, Carabe et al and Chen and Ahmad estimate RBE values that are higher than the experimental mean but give predictions within one standard deviation for most of the measurement points. The RMF predicts lower RBE values than all other models. However, the estimated values for the RBE are well within error bars for all data points. The track structure model gives RBE estimations even lower than the RMF model

upstream of the SOBP as well as throughout the proximal and central part of the SOBP. The predicted slope of the curve in the distal part of the SOBP and at the distal edge is significantly steeper than predicted by all other models. The amorphous track based MKM produces the smallest rise in RBE throughout the SOBP [48].

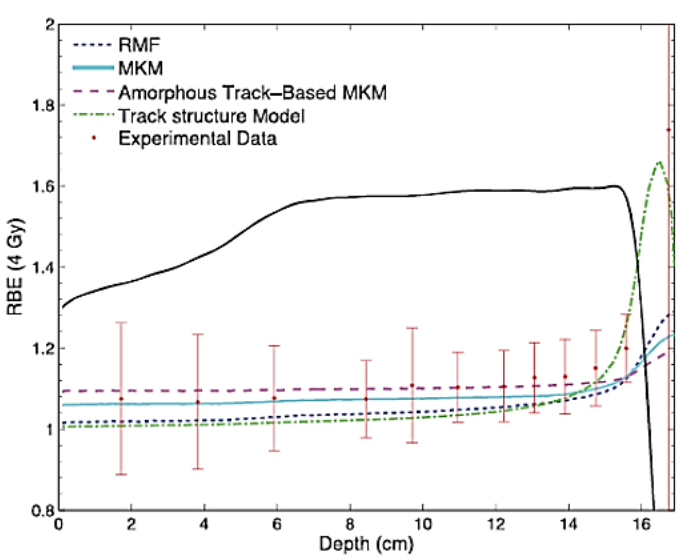

Figure 4.7: RBE values predicted by non LQ-based models [48].

Chapter 5

5. The FLASH effect depends on oxygen concentration

5.1 Oxygen depletion

Recent in vivo results have shown prominent tissue sparing effect of radiotherapy with ultra-high dose rates (FLASH) compared to conventional dose rates (CONV). As already written in Chapter 3, to nowadays several hypotheses are being investigated to correctly explain the FLASH effect. It has been suggested, among the most relevant theories, that this apparently beneficial effect is due to differences in oxygenation in tumor and healthy tissues. The differential response between FLASH-RT and CONV-RT may be due to radiochemical oxygen depletion at very high doses and the resulting radioresistance conferred on the irradiated tissue. It is largely accepted that hypoxic tissues are more radioresistant than well-oxygenated tissues. This is because in the presence of molecular oxygen there is a fixation of radiation-induced indirect DNA damage. Indirect damage, the predominant mechanism by which low linear energy transfer (LET) radiation induces DNA damage, occurs when the radiation causes radiolysis of water molecules and subsequent generation of free radicals. The free radicals are then incorporated into DNA, causing damage, but this can be easily resolved. However, if a free radical reacts with molecular oxygen, this produces a peroxyl radical. Peroxyl radicals have the potential to induce permanent damage and are therefore a more effective DNA damaging agent. Thus, the lack of oxygen in the immediate environment of a cell limits the extent of radiation-induced DNA damage [30]. When considering oxygen depletion theory, it is important to note the nature of physiologically relevant oxygen concentrations, or *physoxia*. Normal tissues in vivo are perfused at much lower oxygen concentrations than in vitro cell lines cultured in atmospheric oxygen concentrations. Depending on tissue type, physoxia is generally between 3.4 and 6.8% oxygen [50]. The data so far collected suggest that tissue irradiation with FLASH-RT causes radiochemical oxygen depletion, resulting in an extremely acute period of hypoxia within the irradiated tissue and consequently transient radioresistance. This phenomenon does not occur following irradiation with CONV-RT, as the radiation is delivered in much smaller pulses and for a longer period. Thus, during

CONV-RT, oxygen depletion is limited and there is sufficient time for oxygen to diffuse into the irradiated region to replace the oxygen that has been lost. Therefore, the oxygen concentration within the irradiated tissue is maintained [30]. The oxygen depletion hypothesis seems to explain the reduced toxicity of FLASH-RT to normal tissue. However, it does not readily explain how FLASH-RT can maintain the tumor response compared with CONV-RT. Although tumors are more hypoxic than their normal tissue counterparts, most are not completely anoxic [50]. Therefore, after FLASH-RT, there will also be radiochemical oxygen depletion within the tumor, so this would be expected to confer radioresistance to the tumor. To further investigate this aspect as well, it would be interesting to compare the DNA repair capacity of normal tissue versus tumor tissue: it is thought that the radioresistance induced in tumor tissue by oxygen depletion is compensated by a lower DNA repair capacity than in normal tissue. Therefore, regions of hypoxia occur in most solid tumors in contrast to the physiology found in the surrounding normal tissue. This could be relevant to the relative repair of FLASH-RT-induced DNA damage, as exposure to hypoxia has also been described to cause repression of DNA repair pathways [30].

5.1.1 Water radiolysis

FLASH radiotherapy delivers a high dose (≥10 Gy) at a high rate (≥40 Gy/s). In this way, particles are delivered in pulses as short as a few nanoseconds. At that rate, intertrack reactions between chemical species produced within the same pulse may affect the heterogeneous chemistry stage of water radiolysis [51].

When chemical reactions of reactive oxygen species (ROS) induced by radiolysis are considered, the assumption of independence still applies because the time lapse of the non-homogeneous chemical stage of each history (10^{-7}–10^{-6} s) is much shorter than the time delay between subsequent histories (conventional dose rates are ≤0.03 Gy/s). The likelihood of the ROS created by one history reacting with the ROS created by another is negligible in clinical or environmental exposures. ROS are scavenged within nanosecond (ns) in cells, and the heterogeneous chemistry of radiolysis ends within the first microsecond after the initiating radiation interaction [51].

More specifically about water radiolysis: an ionizing radiation strikes an H_2O molecule

$$H_2O + hv \text{ (or } ½\ mv^2) = H_2O^+ + e$$

With H_2O^+ positive hydride.

The electron hits other water molecules losing energy and slowing down:

$$H_2O + e^- = H_2O^-$$

With H_2O^- negative hydride.

Now there are two chemical species that were not there before: positive and negative hydrides. They are atoms with odd numbers of electrons, they are called free radicals.

Free radicals are highly unstable:

$$H_2O^+ \rightarrow H^+ + OH\cdot$$

A hydrogenion and a hydroxyl radical are formed.

$$H_2O^- \rightarrow H\cdot + OH^-$$

A hydrogen radical and a hydroxyl radical are formed.

Now H^+ with OH^- and H^- with OH^- can combine to give H_2O. However other bonds are also possible:

$$H\cdot + H\cdot \rightarrow H_2$$

From the union of two hydrogen radicals, hydrogen gas is formed hydrogen gas that is released.

$$OH\cdot + OH\cdot \rightarrow H_2O_2$$

From the union of two hydroxyl radicals, it was formed hydrogen peroxide (oxygenated water). Free radicals are unstable and have a short half-life while H_2O_2 is stable for a long time.

Therefore, ionizing radiations can be characterized according to their ability to ionize matter. X-rays and γ-rays are very penetrating but with low ionization density of low density of ionization, while the radiations corpuscular radiation (α, β, protons and neutrons), less penetrating at the same energy, are considered to have a high density of ionization. The magnitude that expresses the energy transferred from the radiation per unit of path in the absorbing medium is called linear energy transfer (LET acronym of "Linear Energy Transfer" or also "collision-restricted linear restricted for collisions") and is measured in keV/μm. Consequently, a high-LET radiation yields considerable amounts of energy in a short path, presents a greater biological effect and a minimal ability to

penetrate the tissues (because it loses its energy in short distances). High-LET radiation may cause several ionizations within a single cell, leading to damage. Ionizations of radiation with low LET in because the energy is distributed over many cells do not cause significant damage.

So, the X-rays or γ-rays have low probability to interact with the atoms and determine, therefore, a low ionization density. The number of free radicals that are formed per mass unit and therefore the relative probability that they will have to meet will be modest. A corpusculated radiation (e.g., a proton) on the other hand has a high probability of interacting with the atoms of matter with relative high density of ionization of ionization and higher probability of formation and combination of free radicals [52].

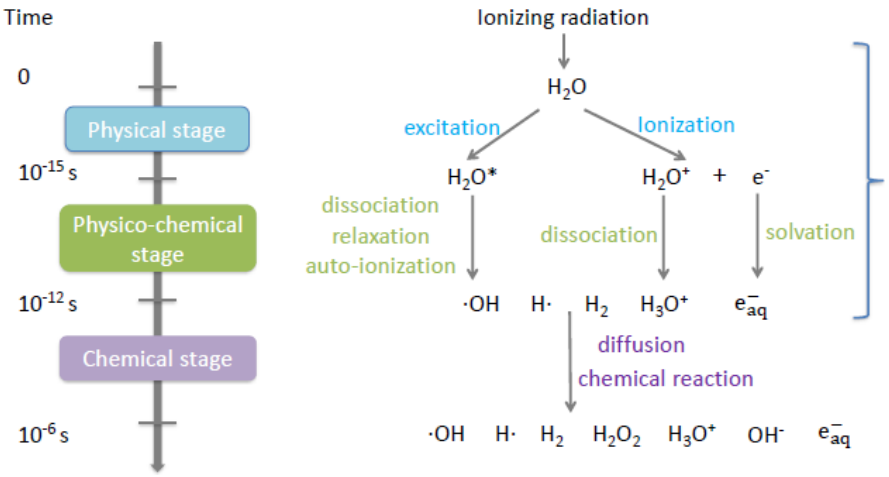

Figure 5.1: Water radiolysis scheme [62].

5.2 Oxygen depletion modelling

Despite studies on the topic, it remains to be understood how such a mechanism succeeds in maximizing the FLASH effect. To this end, several models on the kinetics of oxygen during irradiation have been realized to develop a time-dependent model on the behaviour of oxygen. This model aims to analyse, in terms of dose and dose-rate, the oxygen enhancement because of the therapy. The kinetics of oxygen under high dose and high-rate irradiation have been previously studied in several systems and are used as the basis of a simplified model of O_2 availability. In this context, it is thus imperative to introduce a new parameter, called OER. OERs are typically specified as a simple sigmoid function of the environmental oxygen level. A number of parameterizations are used, with among the most common being:

(5.1)

$$OER = \frac{K + mO_{env}}{K + O_{env}}$$

where m is the maximum OER (typically ≈ 3), and K is the oxygen tension at the midpoint of the OER curve. However, this assumes that the oxygen level does not vary significantly throughout the exposure. If it does, it must instead consider how the OER varies as a function of time and integrate this throughout the irradiation to generate an averaged OER. Specifically, the averaged OER for a dose delivered at a constant rate of $\dot{D}$ for a time T can be expressed as:

(5.2)

$$\overline{OER} = \frac{1}{T}\int_0^T \frac{K + mO(t)}{K + O(t)}\,dt$$

where T is the total time of the irradiation, and O(t) is the time-varying oxygen concentration as defined earlier. This approach assumes that damage caused by irradiation is determined by the oxygen concentration now it is delivered. At least, the exact value of OER is a complex function depending on the interplay between the initial oxygen level, the dose rate, and the total dose delivered (via the exposure time T) [53].

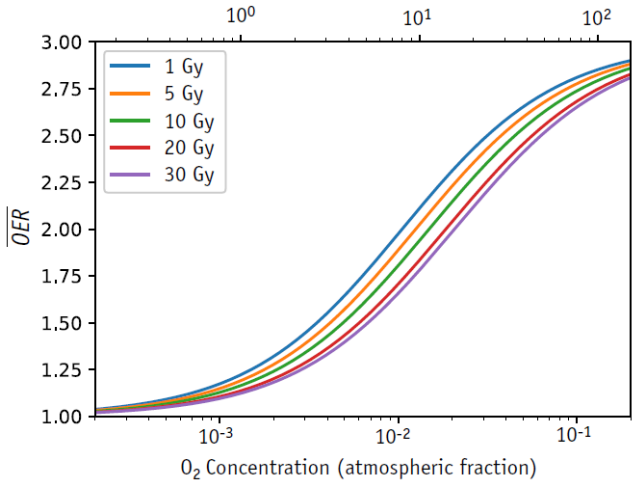

Figure 5.2: Variation in OER for a dose of 15 Gy delivered at different dose rates, for different initial oxygen level [53].

The model just described is a simplified one because, at the biological level, neither oxygen depletion nor oxygen recovery is driven by single mechanisms such as those

described. Higher-order contributions from processes such as superoxide dismutation or radical-radical recombinations in lipids may alter the overall kinetics of oxygen in irradiated systems. Similarly, there may be other differences, currently unaccounted for, in the types of genetic damage caused at ultra-high dose rates that cannot be definitively excluded in the present analysis. However, from this model, observations can be made about the effects of oxygen depletion in FLASH [53]:

1. The FLASH effect depends on a combination of high dose and dose rate. Even in the absence of oxygen recovery, a sufficient dose is required to deplete available oxygen. In addition to this, sufficiently high dose rates are required to deplete available oxygen faster than it can be recovered. The exact thresholds for dose and dose rate depend on the kinetics of oxygen within the system.
2. It is the total dose rate for the entire exposure, rather than the instantaneous dose rate, that is of relevance in driving oxygen depletion relevant to FLASH effects.
3. Preservation of antitumor efficacy in vivo may be driven by the hypoxic core commonly seen in xenograft tumor models. Many tumors have a median oxygen tension of less than 1% (7.6 mm Hg), and almost all xenografted tumors have a significant fraction of fully hypoxic cells with negligible residual oxygen. These resistant hypoxic cells are thought to represent many cells that survive irradiation and lead to tumor recurrence [53].

5.3 Monte Carlo simulation in FLASH therapy

At this point, it becomes apparent how important it is to mechanistically model the effect of oxygen in the water radiolysis process to fully understand how FLASH radiation therapy works. However, due to the computational costs of many-body interaction, oxygen is often ignored in simulations with common microscopic Monte Carlo tools. Instead, in the next chapter, after a brief introduction on the MC method, a MC modelling scheme that take oxygen into account and thus allow for the analysis of the oxygen depletion phenomenon will be explored.

5.3.1 Introduction to MC method

Monte Carlo method is a broad class of computational methods based on random sampling to obtain numerical results. It can be useful to overcome computational problems associated with exact tests (e.g., methods based on binomial distribution and

combinatorial calculus, which for large samples generate an excessive number of permutations). The method is used to derive estimates through simulations. It is based on an algorithm that generates a series of uncorrelated numbers, which follow the probability distribution that is supposed to have the phenomenon to be investigated. The non-correlation between the numbers is ensured by a chi square test. The simulation Monte Carlo calculates a series of possible realizations of the phenomenon in examination, with the proper weight of the probability of such eventuality, trying to explore in dense way all the space of the parameters of the phenomenon. Once calculated this random sample, the simulation executes of the measures of the largeness's of interest on such sample. The simulation Monte Carlo is well performed if the average value of these measures on the realizations of the system converges to the true value [54].
Monte Carlo helps:

- To verify a theory if physics models are in development;
- To develop or verify an experiment in the other case.

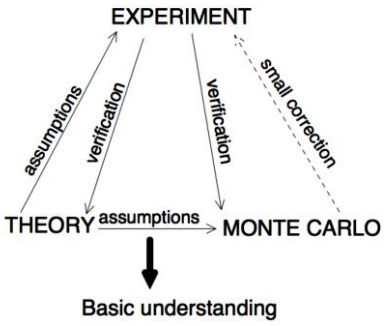

Figure 5.3: Principles of MC [55].

In particle transport, if particles interaction models are known, MC can be used to calculate the parameters of the motion equations in each configuration. Particles are tracked one-by-one, step-by-step and, after a reasonable number of particles, the correct information can be extracted. The Monte Carlo is very time consuming but sometime necessary and with many advantages.

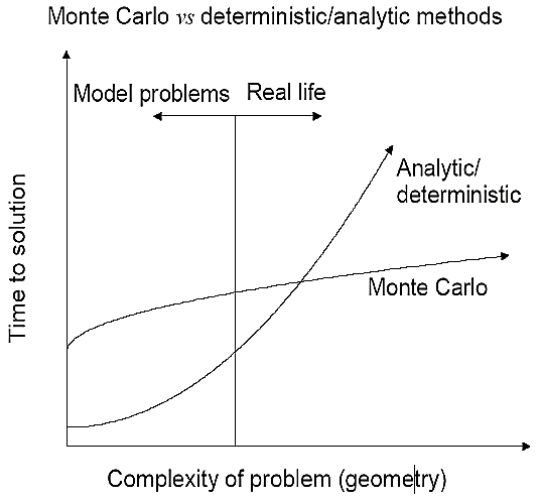

Figure 5.4: Monte Carlo vs deterministic methods [55].

Mathematical proofs exist demonstrating that: MC is the most efficient way of estimate quantity in 3D when compared to first-order deterministic method [55].

GEANT4

The Virtual Monte Carlo (VMC) provides the abstract interface to the Monte Carlo transport codes: GEANT 3.21, Geant4, and FLUKA. The user VMC based application, independent from the specific Monte Carlo codes, can be then run with all supported simulation programs. New developments in Geant4 VMC are mostly driven by the evolution of Geant4 on one side and the requirements from users on the other side. They are presented in two subsections: non physics developments and developments related to user physics selections [56].

GEANT4 is written in C++, is object-oriented and is a toolkit, i.e., a set of tools that the user can use for their own simulation.

Geant4 is a toolkit for simulating the passage of particles through matter. It includes a complete range of functionality such as tracking, geometry, physics models and hits. The physics processes offered cover a comprehensive range, including electromagnetic, hadronic and optical processes, a large set of long-lived particles, materials and elements, over a wide energy range starting (from 250 eV to TeV). Geant4 is driven by the software needs of modern experiments. A typical software system contains components – event generator, detector simulation, reconstruction and analysis – that can be used separately or in combinations. The toolkit has been built as the basis for the simulation component [57]. Thus, it was required:

- To have well defined interfaces to others components;
- To provide parts to be used by the others components.

The key domains of the simulations of the passage of the particles through matter are:

- Geometry and materials;
- Particle interaction in matter;
- Tracking management;
- Event and track management;
- Visualisation and visualisation framework;
- User interface.

These domains naturally led to the creation of class categories with coherent interfaces and, for each category, a corresponding working group with a well-defined responsibility [57].

List of main tools:

- Geometry → It is an analyser of the physical arrangement of the experiment, including detectors, and considers how this arrangement will affect the path of particles in the experiment.
- Tracking → It is a simulator of the passage of particles through matter. This involves consideration of possible interactions and decay processes.
- Detector response → It records when a particle passes through detector volumes and, approximately, how a real detector might respond.
- Run management → It records the details of each run (a set of events), as well as how an experiment is set up in different configurations between runs [57].

GEANT4 is used in static conditions, for this the Geant4-DNA project proposes to develop an open-source simulation software based and fully included in the general-purpose Geant4 Monte-Carlo simulation toolkit. The main objective of this software is to simulate biological damages induced by ionizing radiations at the cellular and sub-cellular scale [58]. GEANT4-DNA is used for the simulation because, unlike GEANT4, it allows for the molecular representation of water.

The Geant4-DNA extension set currently covers the dominant interactions of light particles and ions including electrons, protons, hydrogen, helium particles and their

charged states down to the electronvolt scale in liquid water, the main component of biological matter [58].

Despite this, it remains computationally very expensive to use, so recently has been developed another toolkit, always based on the MC method, called gMicroMC.

This code is the code that I used to perform my simulations and that will be presented in the next chapter, along with the results of my work.

Chapter 6

6. Practical application of Monte Carlo method using gMicroMC code

6.1 Introduction

When ionizing radiation interacts with water, energy transfer by a series of energy deposition events in the physical stage results in ionization or excitation of the water molecules. These physical events lead to direct damages to the DNA. The highly unstable molecular ions and excited water molecules then generate many free radicals in the physicochemical stage. In the subsequent chemical stage, diffusion and mutual chemical reactions of the radicals generate further damages to the DNA. These initial DNA damages caused by ionizing radiation trigger subsequent biological processes [59].

Computing the DNA damages caused by radiation is of central importance for understanding radiobiology and for quantitatively testing hypotheses regarding radiobiological effects. Monte Carlo simulation is one of the most widely used approaches for computations of water radiolysis process and DNA damages. Based on fundamental physics and chemistry principles, the MC method can precisely calculate the time-dependent behaviour of energy deposition by a particle, the reaction-diffusion process of radicals, and their damages to DNA using probabilistic methods. Estimations on the spectrum of DNA damages using MC simulations have played an indispensable role in understanding radiation-induced biological effects in organisms, nonetheless, one of the major factors impeding the use of these MC tools is computational efficiency. Although MC simulations of the physical and physicochemical stage are relatively fast, it takes much longer time for the chemical stage, because of the substantially longer time span of this stage than the other two stages. Furthermore, these radicals diffuse and react with each other, as well as with surrounding background water molecules [59]. For this, a possible solution is to use a GPU-based microscopic MC tool called gMicroMC, developed at Innovative Technology of Radiotherapy Computation and Hardware (*iTORCH*) laboratory, Department of Radiation Oncology, University of Texas Southwestern Medical Center, Dallas, by Dr. Xun Jia and his team.

Instead of developing and implementing new physics or chemistry models, which have been extensively studied over the years by many groups, their focus is developing novel implementations of these models on the GPU platform, such as designing GPU-friendly parallelization schemes, to achieve a high computational efficiency [59].

The code is composed of three parts because it simulates the three phases of radiolysis of water. As previously mentioned, water radiolysis is the process when ionizing radiation interacts with water and inducing the dissociation of water molecules. The accurate modelling of the interactions between water and radicals are of central importance to understand the radiobiological mechanisms and quantitatively test some hypotheses in related radiation chemistry problems. The radiation action of an ionizing particle in water is usually divided into three more or less overlapping stages: physical ($\sim 1\ fs$), physic-chemical ($\sim 1\ fs$ to $1\ ps$) and chemical stage ($\sim 1\ ps$ to $1\ \mu s$) [61].

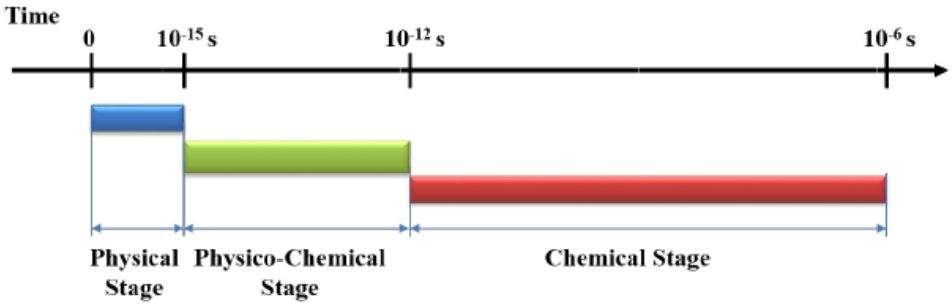

Figure 6.1: Time scale of stages in water radiolysis [61].

Physical stage

In the physical stage, an electron undergoes different types of physical interactions, until its energy falls below a cut-off level. In gMicroMC, it used a step-by-step simulation scheme to transport the initial electron, and all subsequently generated secondary electrons. It considered four types of interactions between water molecule and electrons: ionization, excitation, elastic collision, and dissociative electron attachment and it employed the relativistic extension of the binary-encounter-Bethe (rBEB) model to compute ionization cross sections of electrons with water molecular orbitals for energy range from 10 eV to 100 MeV. The energies were considered for excitation levels of A1B1, B1A1, Rydberg A + B, Rydberg C + D and diffusion [59].

More specifically, during ionization the code considered:

- Five ionization shells: $1b_1$, $3a_1$, $1b_2$, $2a_1$, K-shell;

- Relativistic binary encounter Bethe model(BEB);
- Energy loss: Composition sampling method.

During excitation:

- Five excited states : A1B1, B1A1, Ryd A+B, Ryd C+D, diffuse bands;
- A semi analytic model.

Finally, about elastic scattering:

- < 200 eV: a semi empirical parameterization method;
- > 200 eV: Rutherford cross section with a screening parameter [60].

For the modelling of elastic collisions, the cross sections were given by a parameterized expression with adjustable parameters determined by fitting to experimental data at various incident energies for energies below 200 eV.

Prechemical stage

During this stage, the types and locations of initial radiolytic chemical species entering the subsequent chemical stage were determined. It adopted a simulation including the pathways of ionized and excited water molecules and the thermalization of hot dissociation fragments and sub-excitation electrons. Specifically, ionized water molecules were assumed to undergo dissociation as the sole pathway. Excited water molecules had three possible pathways, relaxation, dissociation and auto-ionization, depending on the excitation type.

After determining a pathway according to the branching ratio, the hot dissociation fragments had to be thermalized by getting rid of kinetic energy released in the dissociation process. The decay channels and the corresponding branching ratios used in the package are shown in Table 6.1.

		Pathway	Decay channel	Branching ratios (%)
Ionized water molecules	$1b_1$, $3a_1$, $1b_2$, $2a_1$, K	Dissociation	$H_3O^+ + \cdot OH$	100
Excited water molecules	A^1B^1	Dissociation	$\cdot OH + H\cdot$	65
		Relaxation	$H_2O + \Delta E$	35
	B^1A^1	Auto-ionization	$H_3O^+ + \cdot OH + e^-_{aq}$	55
		Dissociation	$H_2 + \cdot O\cdot$	15
		Relaxation	$H_2O + \Delta E$	30
	Rydberg A + B, Rydberg C + D and diffusion	Auto-ionization	$H_3O^+ + \cdot OH + e^-_{aq}$	50
		Relaxation	$H_2O + \Delta E$	50

Tab. 6.1: Branching ratios for ionized and excited water molecules used in gMicroMC [59].

Chemical stage

The chemical stage of water radiolysis consists of two types of chemical kinetics: diffusion of the radiolytic molecules e_{aq}-, ·OH, H·, H_3O+, H_2, OH-, and H_2O_2 and their mutual chemical reactions. Brownian motion was used to model the diffusion of the radiolytic molecules with each being considered as an individual Brownian object with random independent motions. All the chemical reactions considered in this package were assumed to be diffusion-controlled. A reaction would occur, when the distance of the reactants was no greater than the reaction radius [59].

DNA damage calculation

The model used to describe the DNA structure inside a lymphocyte cell nucleus was constructed in a multi-scale fashion with its structure described at six scales. From the finest to the coarsest scale, they were nucleotide pair, DNA double helix, nucleosome, chromatin fiber loop, chromatin fiber unit, and finally the cell nucleus.

The particle and radical transport simulations resulted in locations and types of physics events, as well as locations of radicals at the end of the chemical stage. The code overlapped these physical events and radical locations with the DNA geometrical model to compute DNA damages of different complexities. The computation included two major steps. The first step was to calculate strand breaks (SBs) caused by physical events (direct damages) or radicals (indirect damages). For the direct strand breaks, it first identified if each physical event fell in a sugar-phosphate group. This was considered true, if the event location was within a distance of R + Rp from the center of the sugar-phosphate group, where R is the radius of the group and Rp is reaction distance taken as the thickness of the first hydration layer, which is ~0.1 nm. If the event fell into multiple groups, the one with its center closest to the event location was chosen. After processing all energy deposition events, gMicroMC aggregated all the energy deposit to each sugar-phosphate group. The strand was considered broken if the deposited energy was over E_{thres} = 17.5 eV. As for the indirect strand breaks, it assumed that only the ·OH radical could lead to a break. The second step of DNA damage calculation was to compute damages of different levels of complexities [59].

6.2 gMicroMC code structure and GPU implementation

The code is composed of the following three sequential parts. The users can run them separately. Notice that the running of physicochemical stage and chemical stage needs to read data from previous stage, namely physics stage and physicochemical stage, respectively. The user may give their own designed data according to the data format needed by those two programs.

Phy_stage is the part for the electron physical transport. Here four components are defined, including the GPU device index, the cut-off energy for the electron transport, the file name for the source configuration and one idle input for possible future use.

Prechem_stage is for the de-excitation of water molecules and *Chem_stage* for the radical diffusion in the chemical stage and the DNA damage analysis.

A GPU that supports CUDA should be installed previously. Program has been tested in Nvidia Quadro P400, Nvidia Titan Xp and Nvidia V100 GPU cards. Ubuntu 16.04 and 18.04 have been tested. CUDA versions of 9.0, 9.2, 10.0, 10.2 have been tested [62].

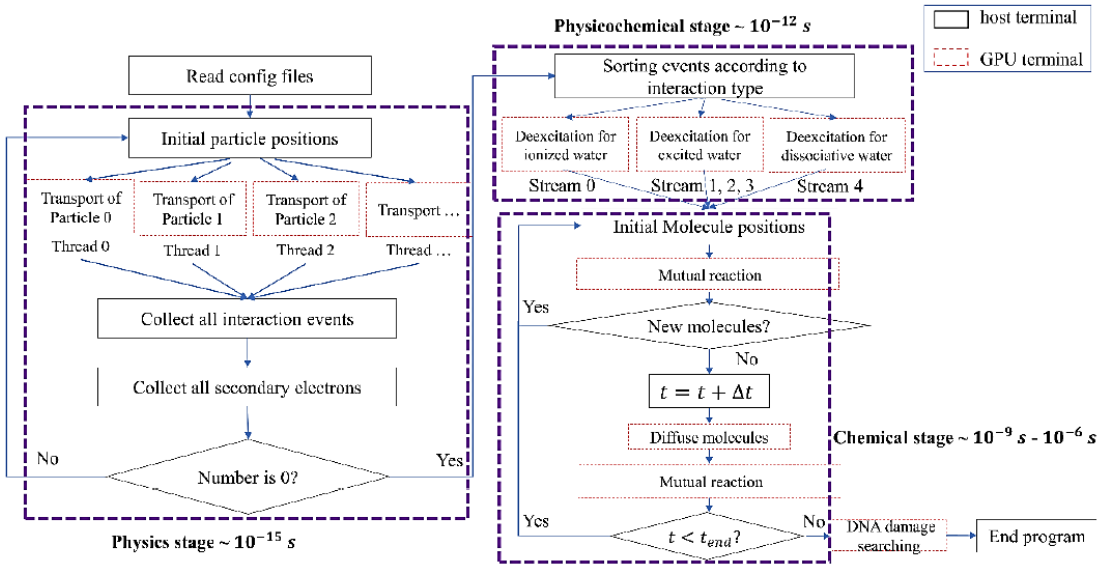

Figure 6.2: Workflow of gMicroMC [63].

Depending on the characteristics of computational tasks, different types of GPU parallelization schemes were employed.

Physical stage: in this stage, each GPU thread was responsible for simulating the transport of one incident or secondary electron. In most applications, there was only one initial electron. However, this initial electron may trigger many secondary electrons. Transport simulation of these secondary electrons was parallelized to enhance the overall

efficiency. In this stage, lookup tables were created to store tabulated data such as cross section data of interactions, cosine values of the deflection angle for the computations in elastic collisions etc. For GPU, reading the data from memory was often faster than computing them using certain algorithms [59].

More specifically, during the physical stage of the code electron iteratively underwent four key operations in the GPU kernel: interaction selection, energy drop, direct deflection and location hop until it is considered as dead (below cut-off energy). Each GPU thread is responsible for simulating the transport of one incident or generated secondary electron. In the interaction select operation, the desired cross section values are checked out from the pre-created lookup tables of all interactions. Cross section values are achieved with linear interpolation according to the current energy. The input energy range for the dissociative attachment cross section goes from 4.3 eV to 12.9 eV with linear scale while in the other interactions, ionization, excitation and elastic, the energy range goes with logarithmic scale from 10 eV to 100 MeV. After summed up the cross-section values checked out from all partial interactions, a random sampling is applied to determine a particular interaction [61].

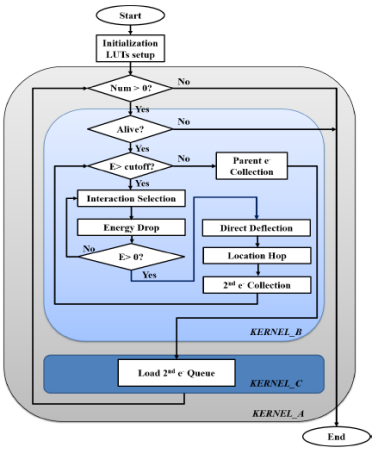

Figure 6.3: Flowchart of the physical stage code implemented with CUDA Dynamic Parallelism [61].

Physicochemical stage: since the pathway of ionized and excited water molecules and the thermalization of sub-excitation electrons are independent, multiple CUDA threads were created for the simulation of these pathways simultaneously [59].

In other words, the species H_2O^+, $H_2O\cdot$ and e- are converted into other chemical species. The positions and radical types of produced particles are stored in the GPU global memory and then shipped to main memory once the kernel execution ends [61].

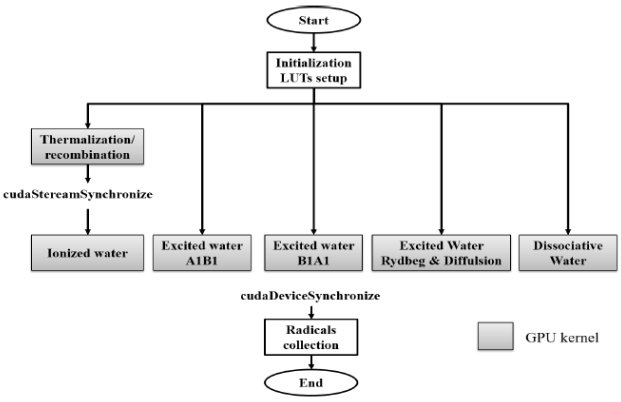

Figure 6.4: Flowchart of the prechemical stage [61].

Chemical stage: during the last stage, by dividing the simulation geometry into grids, the number of possible reactant pairs of molecular species can be reduced. This reduces code complexity and process time for searching pairs of molecular species. The approach requires the update of a lookup table at the beginning of every time step. Each GPU thread is employed for one live molecule to search for potential reactant pairs using the updated grid data. Two conditions to determine whether to simulate a reaction for each pair:

1. A potential pair satisfying their distance does not greater than the reaction radius R, the reaction was simulated.
2. A potential pair satisfying their distance greater than the reaction radius, the thread computed the crossing probability using Brownian bridge method and simulated it if needed [61].

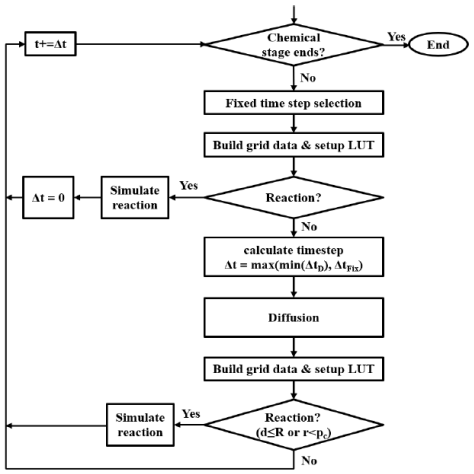

Figure 6.5: Flowchart of one single time step of the gMicroMC chemical stage [61].

6.3 Simulations of water radiolysis process

In the following paragraph will be described the simulations carried out using the toolkit gMicroMC and the results obtained. The working environment used for the code is Ubuntu 16.04, while as hardware architecture the choice has gone to CUDA (Computed Unified Device Architecture) 9.0.

In this thesis work, analysing the process of radiolysis of water, the goal is to evaluate the possible damage to DNA after the use of ionized radiation. To do this, the code simulates the transport of primary electrons during the physical phase of the process, the position of the radicals created during the pre-chemical phase and, finally, their possible reactions with the nucleus during the chemical phase.

6.3.1 Simulation set-up

The physical phase is the only one that requires a configuration step to run the simulation. Within the source.txt file are the parameters needed for configuration. The file looks as follows:

- The first line: Electron simulation history N and a flag (0 and 1) to specify two different configurations. Specifically:
    - Flag = 0, all electrons will be initialized with a kinetic energy E (specified in line 2), within a sphere of radius R (specified in line 3). Their positions and velocity directions will be randomly sampled.
    - Flag = 1, the initial state of the N electrons will be specified in sequential. For each line (starting from line 4) representing one electron, quantities are defined in the order of position (x, y, z), global time t, normalized velocity direction (vx, vy, vz) and kinetic energy (E). Notice, in this situation, lines 2-3 are required to be kept, but the information will not be used.
- The second line: kinetic energy (in eV).
- The third line: spherical radius (in cm).
- The fourth to N+3 lines: each lines contain position (x, y, z, in cm), global time t (in seconds), normalized velocity direction (vx, vy, vz) and kinetic energy E (in eV) [62].

The simulations, carried out by varying some of the most significant parameters of the water radiolysis process, were performed, therefore, on two different sets of electrons:

1. Initialized electrons with kinetic energy Ek, without spheres of radius R and with random direction and velocity. These will be referred to as ***rnd electrons***;
2. Electrons initialized with kinetic energy Ek, R = 65 cm, random direction and velocity oriented along the z-axis. These will be referred to as ***vz electrons***.

I sampled, for each group, one electron at a time in a water sphere containing a human lymphocyte nucleus and transport the electrons and generated radicals until 2 Gy dose was accumulated in the nucleus. I computed DNA damages caused by electron energy deposition events in the physical stage and the hydroxyl radicals at the end of the chemical stage. The most important parameters involved in the simulation are:

a. physics cross section;
b. cut-off energy for electron transport;
c. three branching ratios of hydroxyl radicals in the de-excitation of excited water molecules;
d. temporal length of the chemical stage;
e. reaction radii for direct and indirect damages;
f. threshold energy defining the threshold damage model to generate a physics damage;
g. minimum and maximum energy values defining the linear-probability damage model to generate a physics damage;
h. probability to generate a damage by a radical.

Process	Notation	Description	Default values
Physical	S_{cx}	Scaling factor to change the cross section of electron in water	1
	E_c	Cutoff energy of electrons in water	5 eV
Physicochemical	Γ_1	Probability for dissociation pathway from A^1B^1 excitation status	0.65
	Γ_2	Probability for autoionization pathway from B^1A^1 excitation status	0.55
	Γ_3	Probability for autoionization pathway from Ryd A + B, Ryd C + D, and diffuse bands excitation status	0.5
Chemical	T_r	Temporal length of the chemical stage	1.0 ns
DNA damage analysis	R_p	Reaction radius to search for a direct damage	0.1 nm
	R_c	Reaction radius to search for an indirect damage	0.08 nm
	E_{thres}	Threshold energy value in the threshold damage model for direct damages	17.5 eV
	E_{min}	Minimum energy defining the linear-probability damage model for direct damage	5.0 eV
	E_{max}	Maximum energy defining the linear-probability damage model for direct damage	37.5 eV
	P_r	Probability of a radical to generate an indirect damage	0.4

Tab. 6.2: Summary of parameters studied and the default values for this work [64].

Some of these parameters remained unchanged throughout the duration of the simulations, such as, for example, the cut-off energy of 7.5 eV and the cross section, while others were varied to observe how the response changed. Specifically, I quantified sensitivity of SSB and DSB varying the initial kinetic energy of electrons and varying the temporal length of the chemical stage Tc.

6.3.2 Simulations at variation of initial kinetic energy

For the first type of simulations, I decided to vary the initial kinetic energy of the electrons. The energy range chosen, consistently with the particles treated, goes from 4.5 keV up to 100 keV. Below is table 6.3 with some significant output parameters of the simulations, such as, for example, the duration of the simulation itself and the damage caused to DNA.

Rnd electrons				***Vz electrons***			
Ek (keV)	*Time of simulation (s)*	*Physical damage*	*Chemical damage*	*Ek (keV)*	*Time of simulation (s)*	*Physical damage*	*Chemical damage*
4.5	5.885409	1	1	4.5	14.888740	1	1
9	6.104946	2	2	9	24.458654	0	0
15	6.520722	0	0	15	18.951303	0	0
50	5.747578	0	0	50	9.707108	1	1
100	8.011676	1	0	100	7.514224	7	1

Tab. 6.3: Output parameters for rnd and vz electrons.

By analysing the results obtained from the simulations in MATLAB, it was possible to obtain a 3D reconstruction of the radiolytic molecules generated at the end of the three phases: physical ($t = 1\ fs$, plotted in blue spots), prechemical ($t = 1\ ps$, plotted in orange spots) and chemical ($t = 1\ \mu s$, plotted in yellow spots) stage with a 4.5 to 100 keV incident electron traveling in the z-direction (impact point at x = y = z = 0) produced by the gMicroMC code. This figure can clearly demonstrate the reaction-diffusion process during the chemical stage, while the radiolytic molecules distribution in this stage is more spreads out than others.

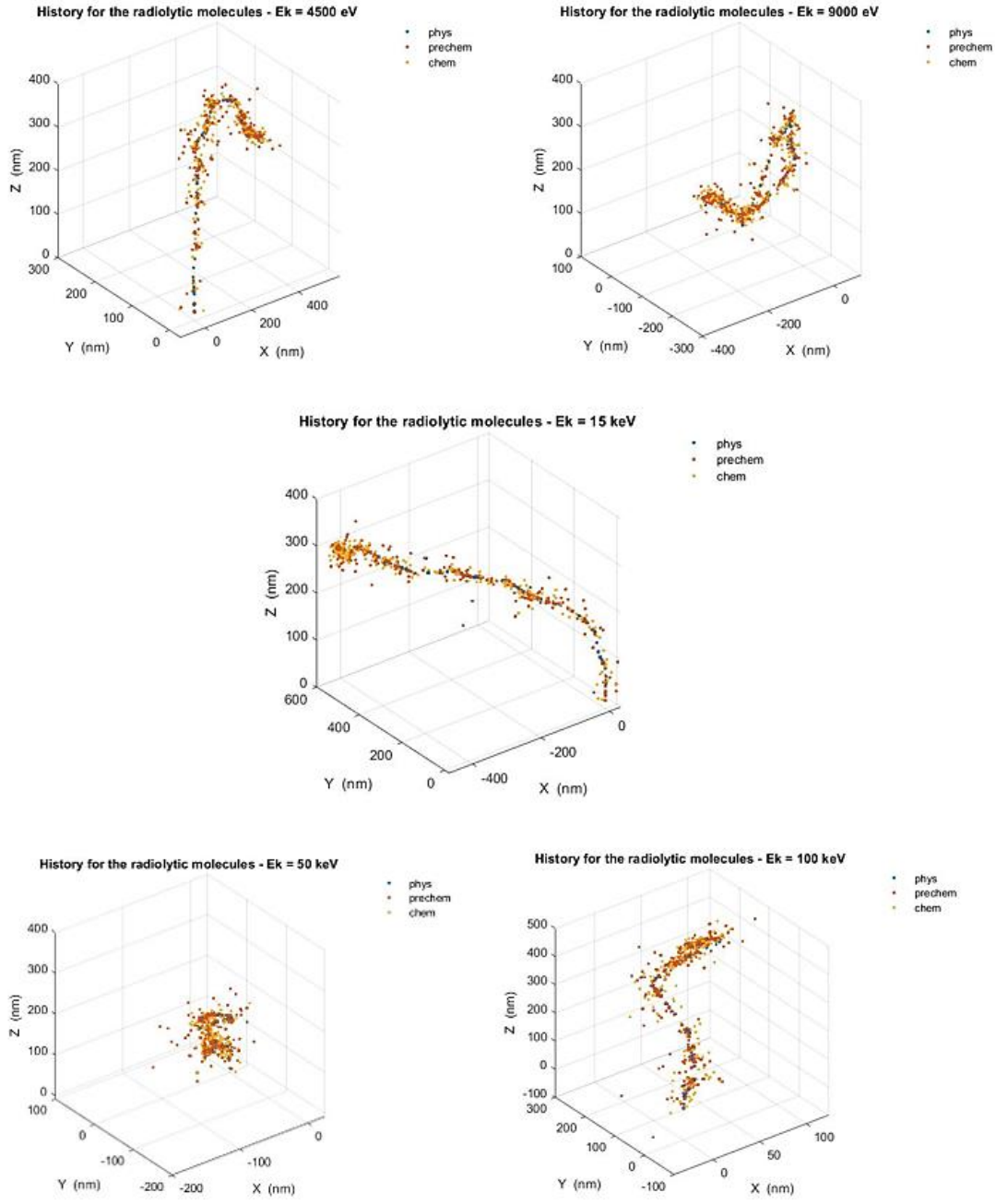

Figure 6.6: History for radiolytic molecules – vz electrons.

At the same time, the same graphs were made for rnd electrons.

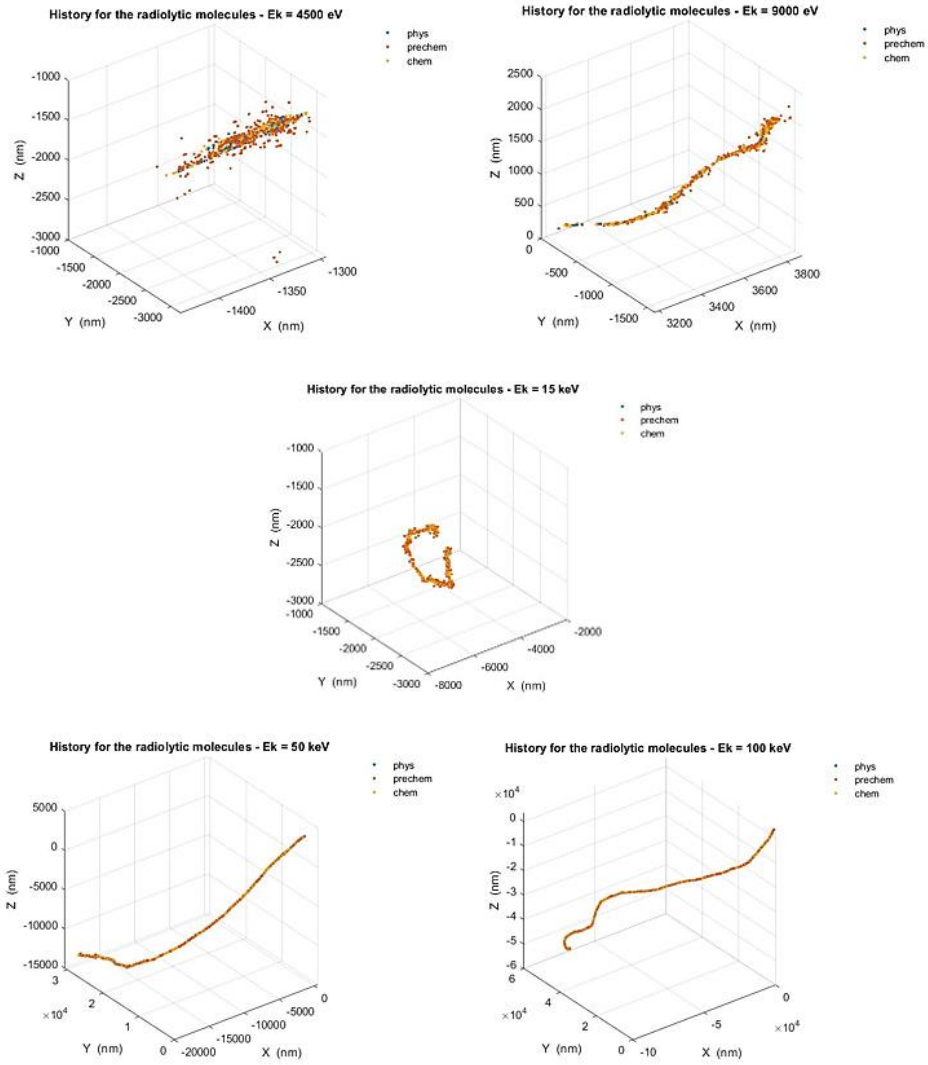

Figure 6.7: History for radiolytic molecules – rnd electrons.

Observing the figures, and through the analysis of the terminals of each simulation, it is evident that as the kinetic energy increases, the number of particles considered increases, although the growth occurs more slowly in the case of vz electrons compared to rnd electrons. In addition, in the case of vz electrons, it can observe a better distribution of molecules, most likely due to the initial direction of the incident electron, the z-direction in the water medium.

The physical phase in the process of water radiolysis plays a key role in DNA damage because it is here that direct and indirect single helix damage is triggered. For this reason, it is interesting to plot, again on MATLAB, the electron deposited energy distribution in

the form of a histogram. Below are the results obtained for both types of electrons considered.

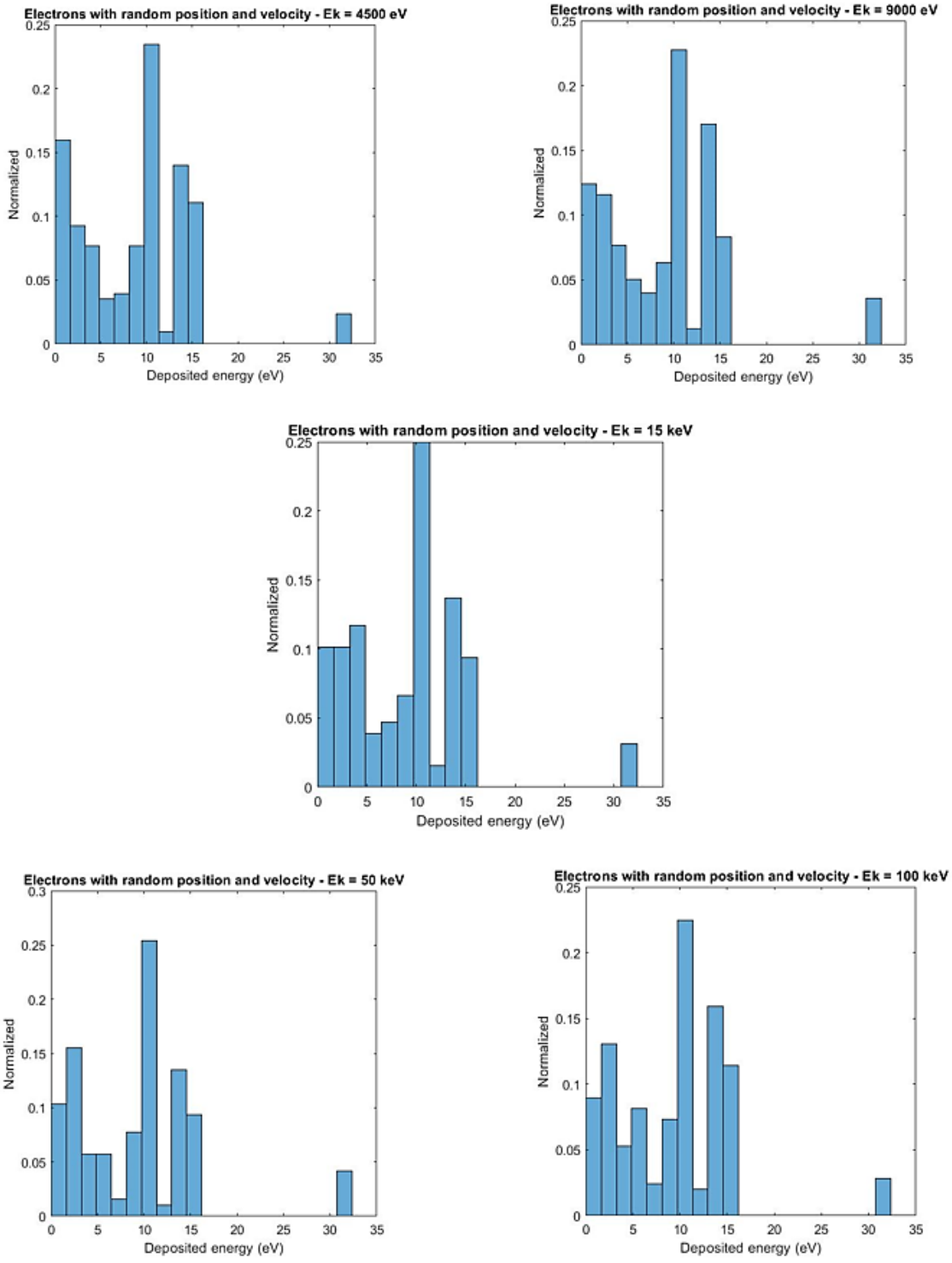

Figure 6.8: Distribution of deposit energy of rnd electrons.

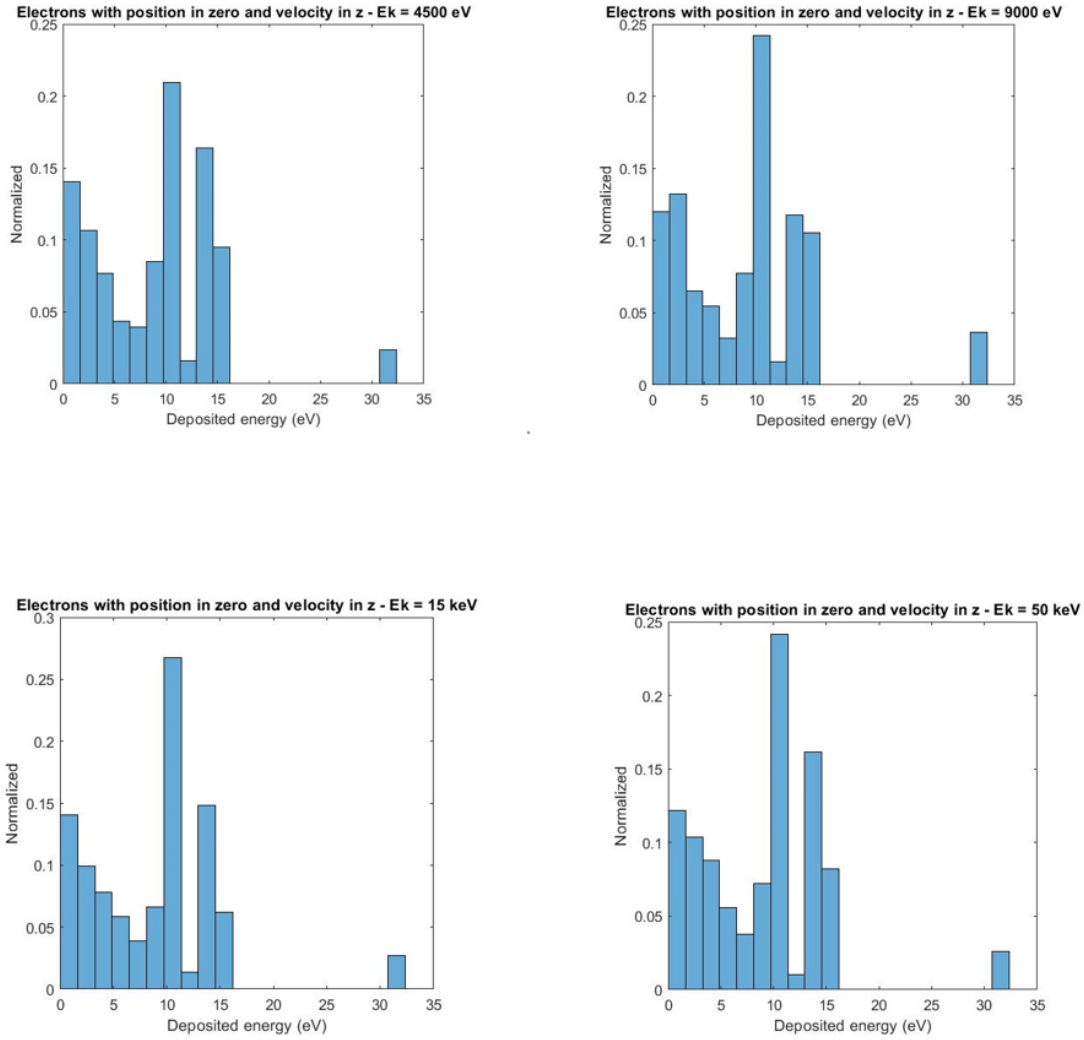

Figure 6.9: Distribution of deposit energy of vz electrons.

As shown in Fig. 6.8 and 6.9, most energy deposit events have energy below 10 eV. Damages are likely generated, only when multiple events are within a sugar-phosphate group, so that the accumulated energy is higher than the threshold. However, only at the very end of the electron track can multiple events be more likely to be in the same group. Hence, reducing physical damages by raising the threshold energy mainly affect DSBs, since the distances between physical events are close in the end of the track.

The results obtained are consistent with those found in the literature. As a matter of fact, below is the histogram (Figure 6.10) for electron energy deposition during the physical phase obtained by the team that developed and tested the code. The comparison has been made for kinetic energy values equal to 100 keV using electrons with speed directed along

the z axis. Comparing the two histograms it is evident that the deposit energy accumulates around the same energy values along the x-axis.

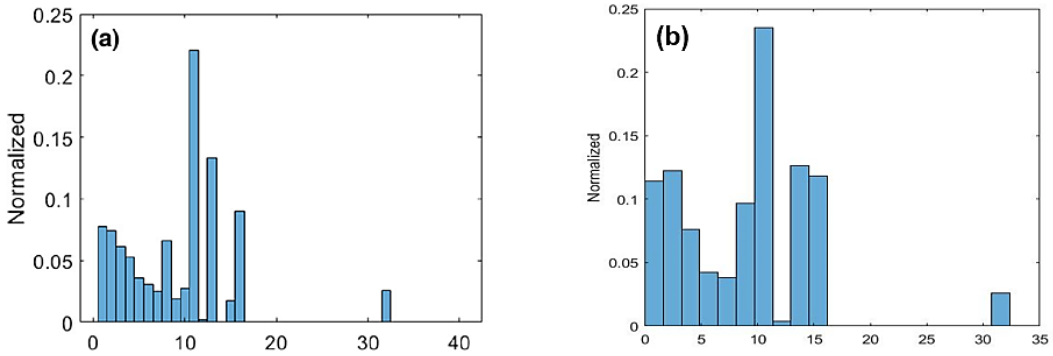

Figure 6.10: Comparison of the two graphs: (a) results obtained in the literature; (b) results obtained from the simulations performed in this work [64].

6.3.3 Simulations at variation of Tc

The second parameter that was varied to observe the response at the end of the simulations is the duration of the chemical phase, denoted as Tc.

Similar to the previous case, again the simulations were performed on the two sets of electrons.

It was decided to consider Tc as a significant parameter of the simulations because, after the radical species are produced at the end of the prechemical phase, they will react with each other through a controlled diffusion process during the chemical phase. Since DNA damage is calculated by superimposing the position of the hydroxyl with the DNA geometry after the chemical phase, it is crucial to go and investigate its length (Tc) because it affects the geometric configuration of the radicals. The range chosen goes from 1ns to 2.5 ns, it does not consider higher values because for Tc > 2.5 ns the Scavenger effect is involved. It talks about Scavenger effect to indicate the formation of substances capable of transforming oxygen free radicals into non-radical compounds, devoid of reactivity and toxicity.

It has been observed, both in literatures and in these simulations, that as the Tc considered increases the SSBs and DSBs decrease. This occurs because the hydroxyl radicals are depleted due to the prolongation of the chemical phase.

It is worth noting that two categories of input data were needed for the chemical stage simulation. One was the basic chemistry data to specify the considered chemical kinetics,

including 1) types of the radiolytic molecules and the diffusion coefficients of them; 2) reaction equations of the chemical reactions and their reaction rate constants.

Because these basic data were small and kept constant during a simulation, they were stored on the GPU's constant memory for fast access.

Species	Diffusion coefficient D ($10^{-9} m^2 s^{-1}$)
e^-_{aq}	4.9
$\cdot OH$	2.8
$H\cdot$	7.0
H_3O+	9.0
H_2	4.8
OH^-	5.0
H_2O_2	2.3

Tab. 6.4: Radiolytic molecule species types and their diffusion coefficients [65].

Another category was the data of radiolytic molecules after the pre-chemical stage, i.e. their types and spatial locations, which were needed because the current gMicroMC package only supports simulations of the chemical stage. It allocated on the GPU's global memory the following memory spaces. First, a molecule array was allocated to record the evolution of the radiolytic molecules during the simulation. This array was initialized with the input molecule data. Second, a chemical reaction considered in the package may produce at most three products. While two of the products can be recorded at the two reactants' locations in the molecule array, an additional space is needed to record the third product. Hence it allocated a buffer array on GPU's global memory. The size of the buffer array was equal to that of the molecule array. Third, it also allocated a tag array associated with the molecule array on the GPU global memory. The function of this array was to inform the GPU regarding the status of each molecule during simulation. Specifically, a tag value of 0 in this array denoted a molecule that had already undergone a chemical reaction and should be excluded from subsequent simulation (referred to as “a dead molecule”). A value of 1 implied that the molecule had not reacted (referred to as “a live molecule”). A value of 2 referred to a new produced at the current time step. It would not be available for reactions until the next time step (referred to as “a new molecule”) [65].

Reaction*	Reaction rate constant ($10^{10}M^{-1}s^{-1}$)
$H\cdot + e^-_{aq} + (H_2O) \rightarrow OH^- + H_2$	2.65
$H\cdot + \cdot OH \rightarrow (H_2O)$	1.44
$H\cdot + H\cdot \rightarrow H_2$	1.20
$H_2 + \cdot OH \rightarrow H\cdot + (H_2O)$	0.00417
$H_2O_2 + e^-_{aq} \rightarrow OH^- + \cdot OH$	1.41
$H_3O^+ + e^-_{aq} \rightarrow H\cdot + (H_2O)$	2.11
$H_3O^+ + OH^- \rightarrow (2H_2O)$	14.3
$\cdot OH + e^-_{aq} \rightarrow OH^-$	2.95
$\cdot OH + \cdot OH \rightarrow H_2O_2$	0.44
$e^-_{aq} + e^-_{aq} + (2H_2O) \rightarrow 2OH^- + H_2$	0.50

Tab. 6.5: Default reaction types and reaction rate constants [65].

As a first step, the trend of radical molecules was evaluated as the input kinetic energy increased and, more importantly, as Tc increased.

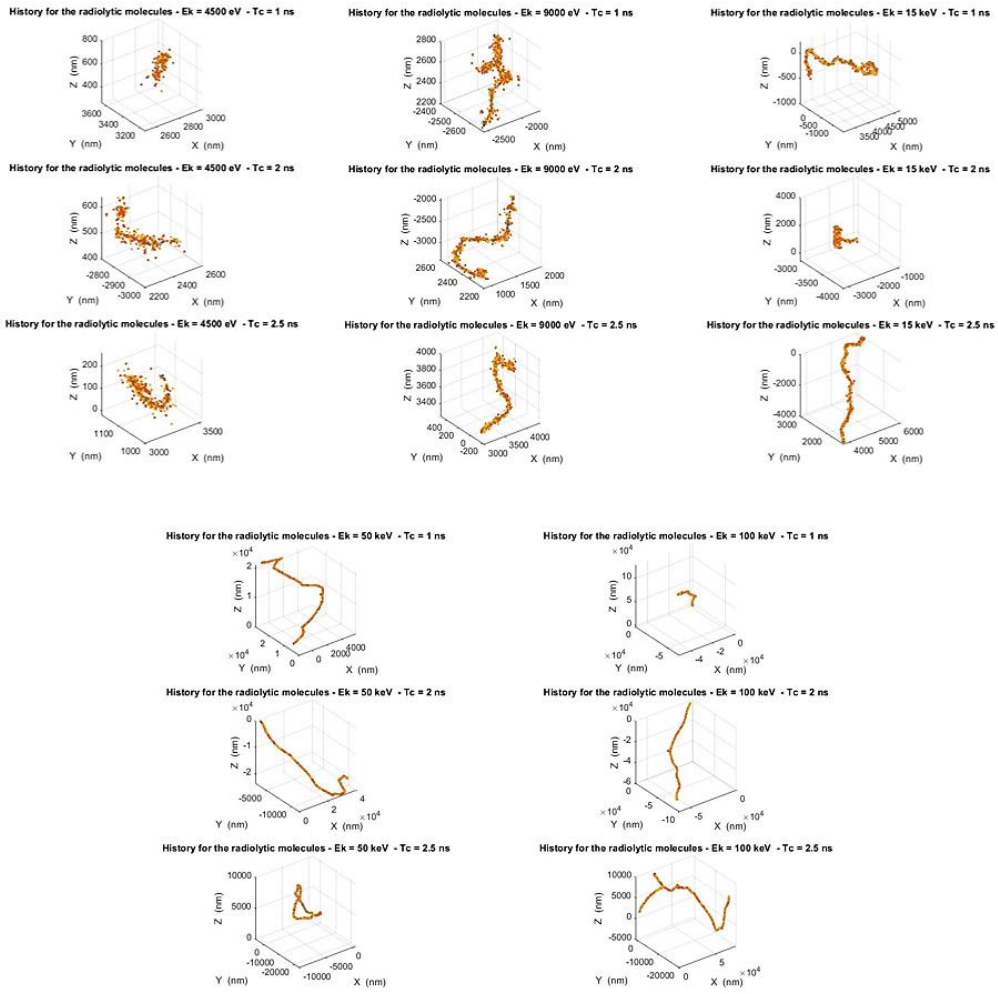

Figure 6.11: History of radiolytic molecules – rnd electrons.

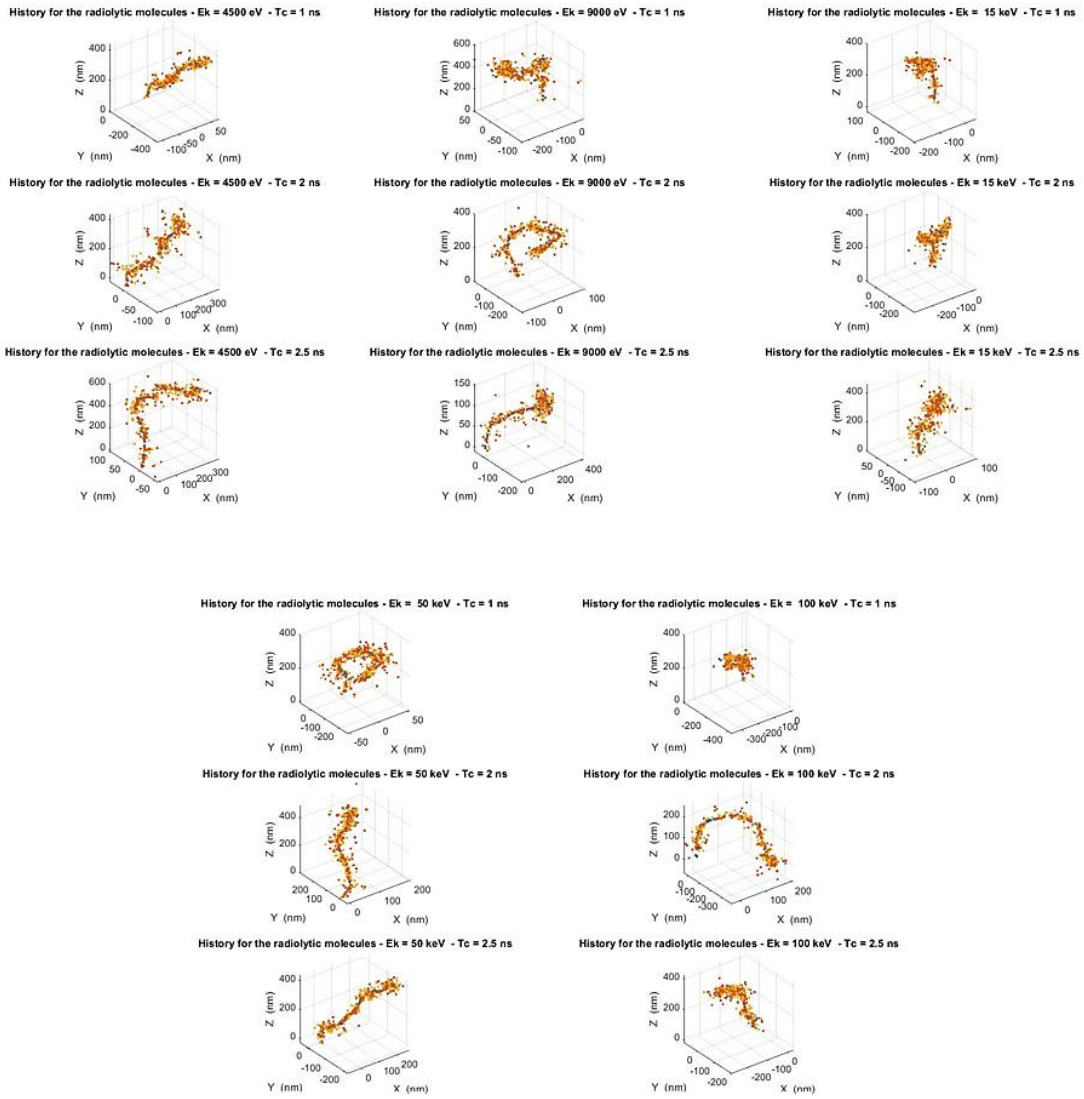

Figure 6.12: History for radiolytic molecules – vz electrons.

The results are similar to those obtained previously, i.e., an increase of the particles considered as the energy increases and a better distribution of the same is observed in the case of vz electrons.

The next step was to analyse in more detail the radical species produced, reported below in the form of histograms.

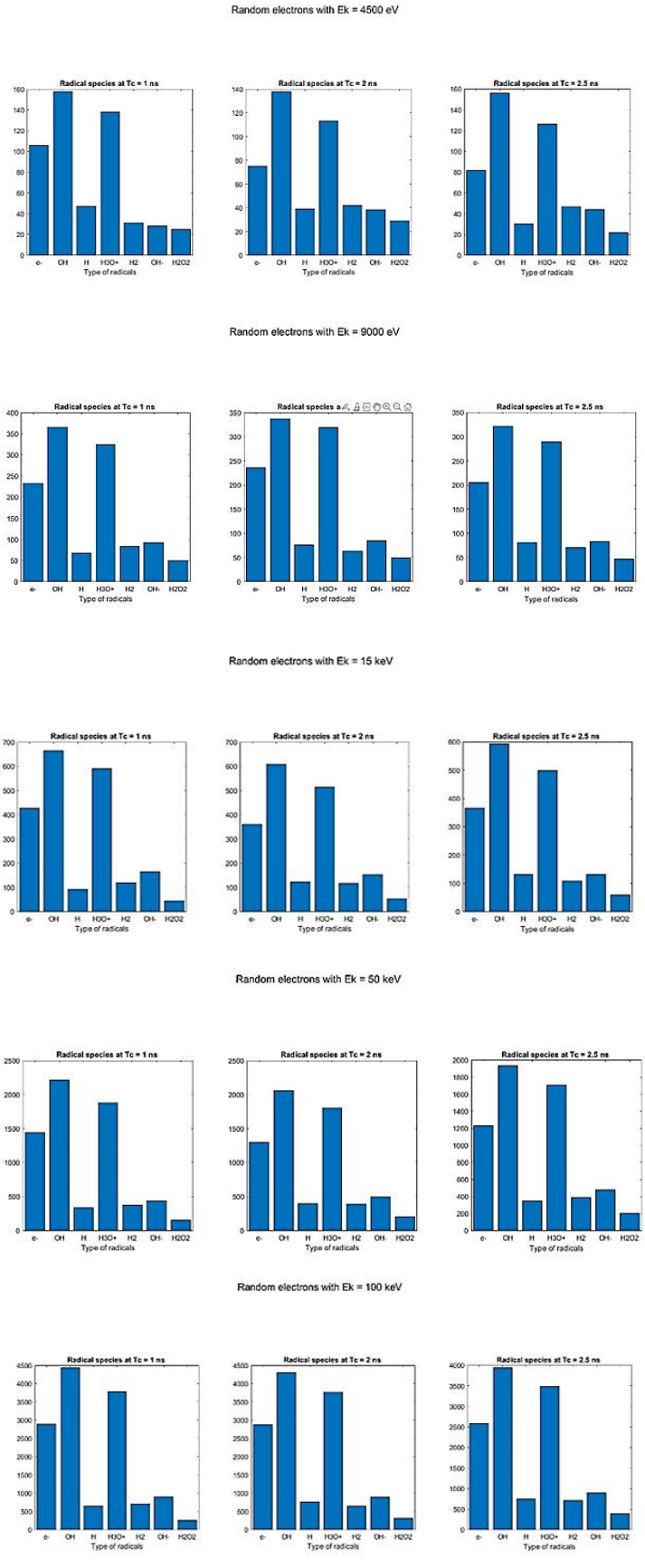

Figure 6.13: Radical species for rnd electrons.

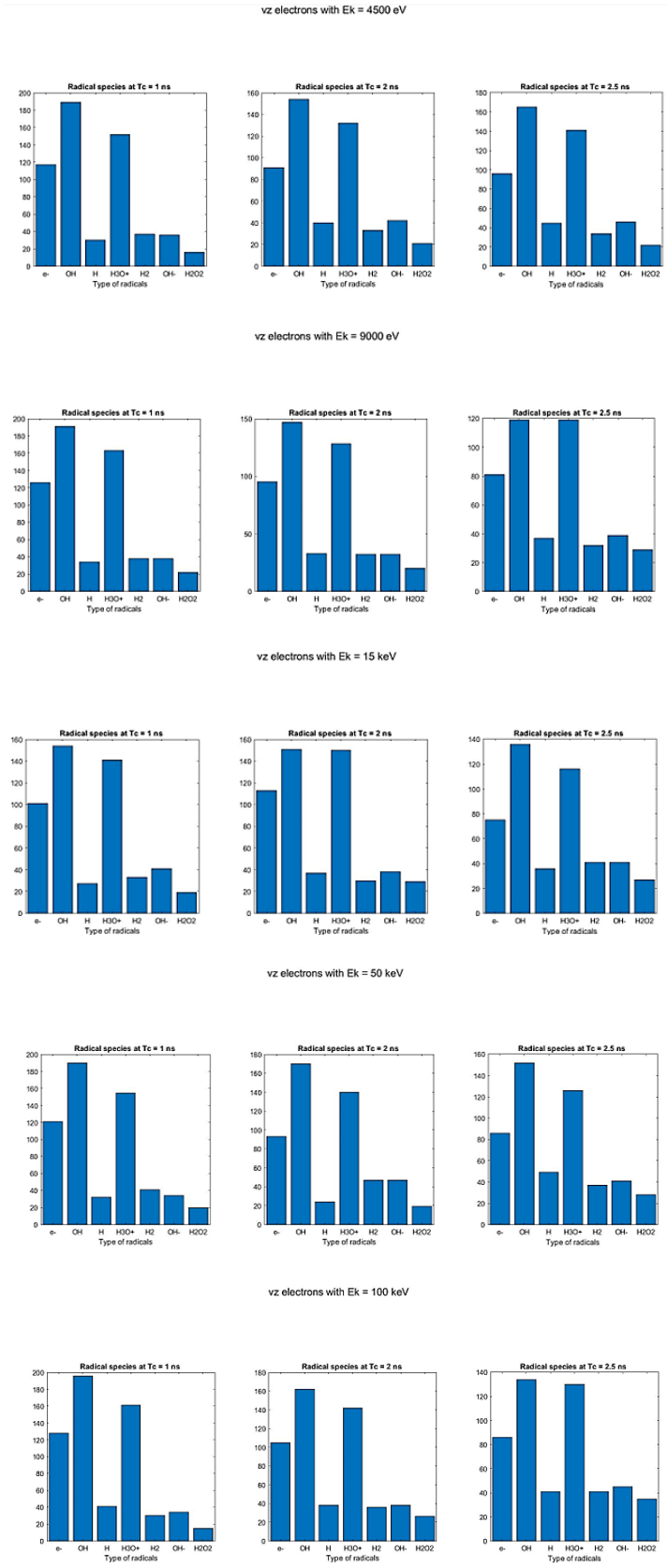

Figure 6.14: Radical species for vz electrons.

gMicroMC calculates the DNA damage formed by radical attack through two successive steps:

1. Radicals react in the chemical phase without DNA;
2. The ·OH coordinates obtained at the end of the chemical phase overlap with DNA. This is referred to as a simplified method or "superposition method".

DNA damage is caused by direct and indirect events. The direct ones have a physical origin, while for the second ones, due to radicals, it is assumed that only ·OHs are able to cause them. Only ·OH hydroxyls are considered because it is known that the rate of reaction between them and DNA is much greater than that of other radicals, which can therefore be neglected.
Moreover, observing the histograms reported in figure 6.13 and 6.14 it is immediately clear that ·OH are among the radicals mostly produced because of the radiolysis process but, at the same time, it can be observed that these tend to decrease as Tc increases.
Therefore, the previous assumption that DNA damage decreases as the duration of the chemical phase increases has been demonstrated.

Finally, to validate the accuracy of the chemical phase it was decided to use the G value. It is a time-dependent radiolytic yield defined as the number of radiolytic molecules produced for a deposited energy of 100 eV in the irradiated medium, formulated as:

(6.1)

$$G(t) = \frac{N(t)}{E/100eV}$$

Where N(t) is the number of molecules per species at time t and E is the total deposited energy in the medium of the incident ionizing particle.
Figure 6.15 shows the trend of G value as a function of chemical phase duration. The graphs refer to vz and rnd electrons with initial kinetic energy equal to 100 keV.

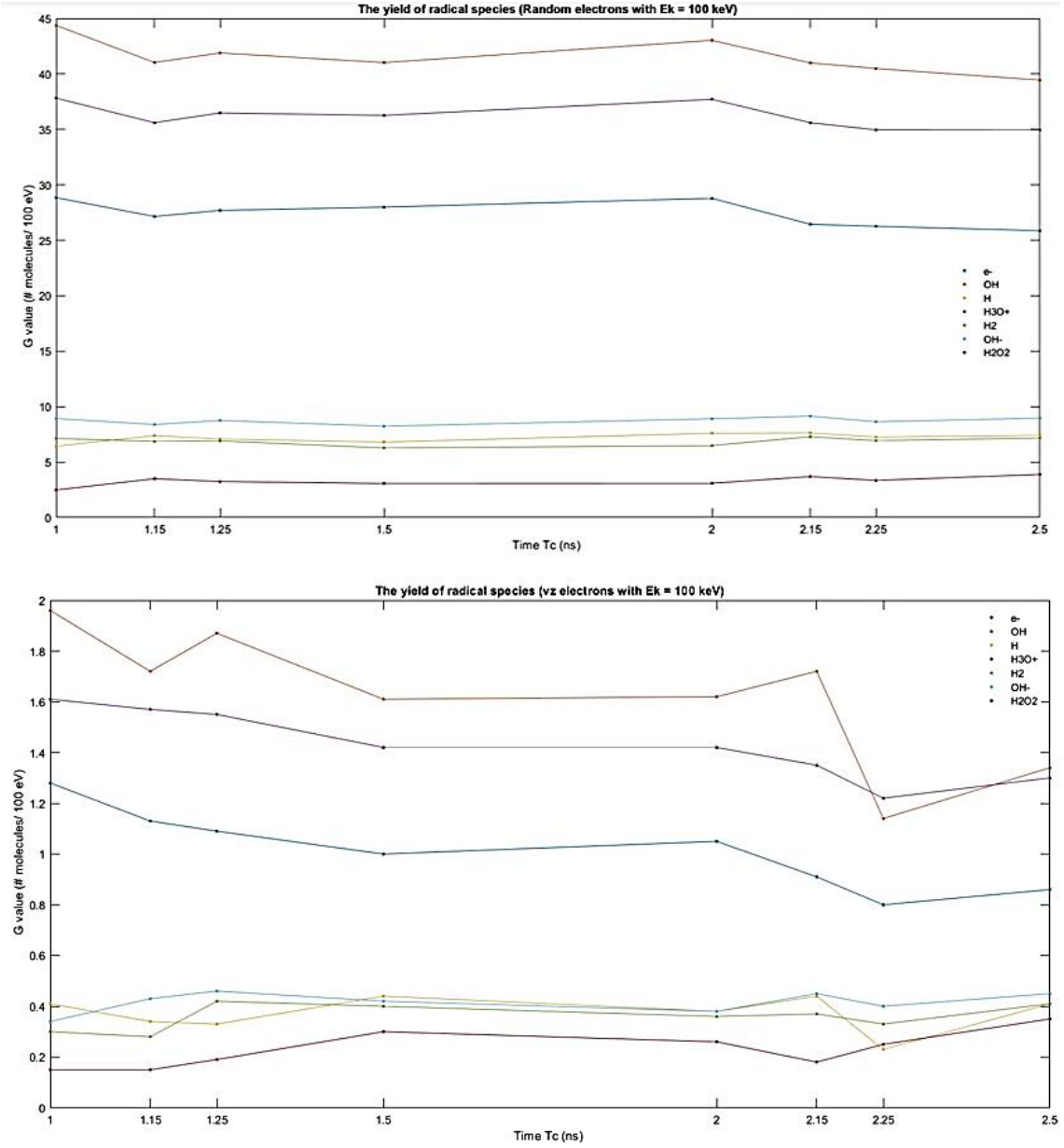

Figure 6.15: Time-dependent yields of species produced in water by a 100 keV electron.

Again, a decrease in ·OH (orange lines) produced can be observed as a function of chemical phase duration.

6.3.4 DNA damage

As mentioned above, the particle and radical transport simulations resulted in locations and types of physics events, as well as locations of radicals at the end of the chemical stage. Overlapping these physical events and radical locations with the DNA geometrical model is possible compute DNA damages of different complexities. The computation included two major steps. The first step was to calculate strand breaks (SBs) caused by

physical events (direct damages) or radicals (indirect damages). The strand was considered broken if the deposited energy was over E_{thres} = 17.5 eV.

As for the indirect strand breaks, it assumed that only the ·OH radical could lead to a break. Hence, for each ·OH radical location, the code searched the DNA structure to find whether it was within a distance of R + Rc from the center of the sugar-phosphate group, where Rc = 0.08 nm is the chemical reaction radius decided by the chemical reaction rate between the radical and the DNA.

Similar to the computations of physical damages, the sugar-phosphate group with its center closest to the radical was selected, if the radical was found to be reacting with multiple groups. After that, the strand break was formed with a possibility Pc of default value 0.4. After processing all radicals, those sugar-phosphate groups damaged by at least one radical were considered as damaged.

The second step of DNA damage calculation was to compute damages of different levels of complexities.

About this, DNA damages are classified based on two factors: based on complexity and based on source/cause. Below is a descriptive table of the various types of damage that can occur at the end of the simulation.

Complexity	***Cause***
No break	SSB_d
SSB	SSB_i
SSB+	SSB_m
2SSB	DSB_d
DSB	DSB_i
DSB+	DSB_m
DSB++	DSB_h

Tab 6.6: Tab. 6.6 Types of DNA damage.

More specifically:

- SSB: one damage on the filament;
- SSB+: two damages on the same filament;
- 2SSB: two or more damages on opposite filaments but sufficiently separated (> 10 bp) not to be considered as double filament breaks;
- DSB: two single-strand breaks on opposite filaments with separation < 10 bp;

- DSB+: double-strand break accompanied by one or more single-strand breaks with separation within 10 bp;
- DSB++: more than one double-strand break.

Regarding causes:

- d: breaks caused by direct damage;
- i: breaks caused only by indirect damage (OH radical);
- m: damage caused by both direct and indirect causes (mixed damage);
- h: we talk about hybrid failure when the damage is caused by a direct failure in combination with an indirect one [66].

Each simulation returns as output a text file, named finalstat.txt, in which the single and double filament damage at the end of the radiolysis process is reported.
Looking at the results obtained, in parallel with what has been seen previously, it can again be stated that DNA damage due to indirect events tends to decrease as the duration of the chemical phase increases.

Conclusions and future prospects

This thesis work is focused on the study of radiotherapy, with particular attention to Hadrontherapy, i.e., the therapy that involves the use of beams of hadrons, particles characterized by a strong interaction. The antitumor effect of Hadrontherapy is greater because hadrons act deeper and are able to deposit high doses of radiation in the tumor limiting the doses to critical organs, even when these are very close to the target.
Therefore, interest in this area is focusing on a technique called FLASH radiation therapy. Unlike conventional radiotherapy (CONV-RT), FLASH-RT delivers a single high dose at an average dose rate of 40 Gy/s in milliseconds to achieve tumor control while protecting normal tissues from damaging injury. It provides an intriguing perspective in improving clinical outcomes for cancer patients, as well as a new way to enhance differential responses between normal and tumor tissues. However, its mechanisms remain largely unclear.
The following are the most widely accepted hypotheses to explain the mechanisms underlying FLASH-RT:

- Oxygen depletion;
- Immune response;
- DNA damage.

The purpose of this work is to investigate primarily the first mechanism, that of oxygen depletion.
It is widely accepted that hypoxic tissues are more radioresistant than well-oxygenated tissues, this is because in the presence of molecular oxygen there is a fixation of radiation-induced indirect DNA damage. Indirect damage, the predominant mechanism by which low linear energy transfer (LET) radiation induces DNA damage, occurs when the radiation causes radiolysis of water molecules and subsequent generation of free radicals. The free radicals are then incorporated into DNA, causing damage, but this can be easily resolved. However, if a free radical reacts with molecular oxygen, this produces a peroxyl radical. Peroxyl radicals have the potential to induce permanent damage and are therefore

a more effective DNA damaging agent. Thus, the lack of oxygen in the immediate environment of a cell limits the extent of radiation-induced DNA damage.

To study this phenomenon, the Monte Carlo method and, in particular, a GPU-based toolkit called gMicroMC was used. The code was used to simulate the behaviour of electrons, in the context then of FLASH with electrons, during the three phases of the water radiolysis process.

Accurate simulation of water radiolysis is an essential step in understanding radiobiological mechanisms and testing hypotheses in related problems. MC simulation of the chemical phase is time-consuming due to the large number of simulation steps required to cover this phase compared to the physical and prechemical phases of water radiolysis. The large number of molecules and the high complexity of the code to track the interactions between them also prolongs the computation, so the focus shifted to gMicroMC, a GPU-based fast microscopic MC simulation package for water radiolysis.

Also, unlike some studies that only consider DNA damage induced by ionization events, all physical events were considered in gMicroMC for two reasons. First, there is a lack of studies on the exact mechanism of physical damage formation in an aqueous environment. Energy deposition events, regardless of ionization, can still cause DNA damage, such as a pressure wave. Second, there are many more ionization events than other excitation events. It would not significantly affect the DNA damage results to consider all physical events.

The simulations carried out, whose results are reported and discussed in Chapter 6, show how, indeed, the process of radiolysis intervenes and is significant during the use of ionized radiation. In addition, it was possible to classify the damage that DNA undergoes and understand, as the parameters involved vary, how these can decrease.

There are several ways that can be pursued in the near future: gMicroMC currently supports only calculations with an electron as initial particle, then the aim will be to add support for calculations of the physical stage of other types of particles, such as protons and heavy ions. This will allow studies of radiobiological effects in different contexts, e.g., carbon ion therapy, space radiation. Second, DNA damage calculations are currently

performed by simply superimposing the trace structure on the DNA geometry as a post-processing step. In fact, the presence of DNA affects the radiation transport, e.g., the scavenger effect, which in turn has an impact on the DNA damage calculation. So, a new implementation of gMicroMC is needed to perform transport simulations considering the existence of DNA structure for DNA damage calculations. It is expected that the simulations will be computationally more demanding, and thus GPU-based calculations will be advantageous.

Bibliography

[1] R. Corvò, F. Grillo Ruggieri, P. Ricci. La Radioterapia Oncologica. *Ruolo, Indicazioni, Evoluzione Tecnologica*, Genova, Omicron Editrice, 2008.

[2] Greco C, Wolden S. Current. Status of radiotherapy with proton and light ion beams. Cancer. 2007 Apr 1;109(7):1227-38. Review. PMID 17326046.

[3] Jones B. The case for particle therapy. Br J Radiol. 2006 Jan;79(937):24-31. Review. PMID 16421401.

[4] M. Durante and J. S. Loeffer. Charged particles in radiation oncology. *Nature Reviews Clinical Oncology* (formerly Nature Clinical Practice Oncology), 7:37-43, 01 2010. doi: 10.1038/nrclinonc.2009.183.

[5] G. Kraft. The radiobiological and physical basis for radiotherapy with protons and heavier ions. *Strahlentherapie und Onkologie: Organ der Deutschen Rontgengesellschaft... [et al]*, 166:10{13, 01 1990.

[6] B. Jones. The case for particle therapy. *The British Journal of Radiology*, 79:24-31, 01 2006. doi: 10.1259/bjr/81790390.

[7] B. Jones. The potential clinical advantages of charged particle radiotherapy using protons or light ions. *Clinical Oncology*, 20:555-563, 2008. doi: 10.1016/j.clon.2008. 02.012.

[8] D. Schulz-Ertner. The clinical experience with particle therapy in adults. *The Cancer journal*, 15:306-311, 2009.

[9] Keith Roberts, Martin Raff, Bruce Alberts, Peter Walter, Julian Lewis and Alexander Johnson. Molecular Biology of the Cell.Garland Publishing Inc, 2008.

[10] Eric Hall. Radiobiology for the Radiobiologist. Lippincott, 2006.

[11] Carlo Martinenghi. Radiobiologia. Cortina Raffaello Ed., 1997.

[12] Maurice Tubiana. Introduction to Radiobiology. CRC Press, 1990.

[13] ICRU 30: Quantitative Concepts and dosimetry in Radiobioloby, 1979.

[14] E.J. Hall., A. Giaccia. Radiobiology for the radiologist.

[15] J. F. Ziegler. *The Stopping and Ranges of Ions in Matter*. Pergamon Press, 1977. ISBN 978-0-08-021605-8,0-08-021605-6.

[16] Lea, D. E., 1946. Actions of radiations on living cells. Cambridge University Press, London.

[17] H. E. Johns, J. R. Cunningham. The physics of radiology.

[18] T. Nomiya. Discussions on target theory: past and present. *Journal of Radiation Research*, 54:1161-1163, 11 2013. doi: 10.1093/jrr/rrt075.

[19] E. L. Powers. Considerations of survival curves and target theory. *Physics in Medicine and Biology*, 7:3-28, 1962. doi: 10.1088/0031-9155/7/1/301.

[20] J. B. Little. Cellular effects of ionizing radiation. *The New England journal of medicine*, 278:369-376, 02 1978. doi: 10.1056/NEJM196802152780705.

[21] J. F. Fowler. Differences in survival curve shapes for formal multi-target and multi-hit models. *Physics in Medicine and Biology*, 9:177-188, 04 1964. doi: 10.1088/ 0031-9155/9/2/305.

[22] B. G. Douglas and J. F. Fowler. The effect of multiple small doses of X rays on skin reactions in the mouse and a basic interpretation. *Radiation Research*, 66:401-426, 05 1976. doi: 10.2307/3574407.

[23] L. M. Coia, D.J. Moylan. Introduction to clinical radiation oncology.

[24] M. Joiner and A. Van der Kogel. Basic Clinical Radiobiology. *A Hodder Arnold Publication*, CRC Press, 4th edition, 2009. ISBN 978-1-4441-0961-0, 978-0-340- 92966-7.

[25] H. D. Thames Jr., H. R. Withers, L. J. Peters, and G. H. Fletcher. Changes in early and late radiation responses with altered dose fractionation: Implications for dose-survival relationships. *International Journal of Radiation Oncology*Biology*Physics,* 8:219{226, 1982. doi: 10.1016/0360-3016(82)90517-x.

[26] G. Luxton, P. J. Keall, and C. R. King. A new formula for normal tissue complication probability (NTCP) as a function of equivalent uniform dose (EUD). *Physics in Medicine and Biology*, 53:23-36, 01 2008. doi: 10.1088/0031-9155/53/1/002.

[27] Ganderson, Tepper (Eds.). Clinical radiation oncology.

[28] S. Salomaa, E. G. Wright. Non-targeted effects of ionising radiation (NOTE) – an ongoing European Integrated project, 2006-2010. *EDP Sciences Journal*. Volume 3-No 5.

[29] Jean Bourhis, Pierre Montay-Gruel. Clinical translation of FLASH radiotherapy: Why and how? *Radiotherapy and Oncology* 139 (2019) 11–17.

[30] Joseph D. Wilson, Ester M. Hammond. Ultra-High Dose Rate (FLASH) Radiotherapy: Silver Bullet or Fool's Gold? *Frontiers in oncology*.

[31] Jonathan R. Hughes and Jason L. Parsons. Review FLASH Radiotherapy: Current Knowledge and Future Insights Using Proton-Beam Therapy. *International Journal of Molecular Sciences*.

[32] Guangming Zhou. Mechanisms underlying FLASH radiotherapy, a novel way to enlarge the differential responses to ionizing radiation between normal and tumor tissues. *Radiation Medicine and Protection* 1 (2020) 35–40.

[33] M. McManus, F. Romano. The challenge of ionisation chamber dosimetry in ultra-short pulsed high dose-rate Very High Energy Electron beams. *Scientific reports*.

[34] R. M. de Kruijff (2020). FLASH radiotherapy: ultra-high dose rates to spare healthy tissue, *International Journal of Radiation Biology,* 96:4, 419-423, DOI: 10.1080/09553002.2020.1704912.

[35] Simon Jolly, Hywel Owen. Technical challenges for FLASH proton therapy. *Physica Medica* 78 (2020) 71–82.

[36] https://www.youtube.com/watch?v=bP6Eve6OUJk

[37] J.S. Loeffler, M. Durante. Charged particle therapy|optimization, challenges and future directions. *Nature Reviews Clinical Oncology* 10, 2013.

[38] A. Carabe-Fernandez et al. Range uncertainty in proton therapy due to variable biological effectiveness. *Phys. Med. Biol*. 57 1159, 2012.

[39] http://www2.pv.infn.it/~altieri/webmail/DISPENSA-05-06/fis-radio-cap7-13.pdf

[40] J J Wilkens, U Oelfke. A phenomenological model for the relative biological effectiveness in therapeutic proton beams *Phys. Med. Biol*. 49 2811, 2004.

[41] M. Wedenberg et al. A model for the relative biological effectiveness of protons: The tissue specific parameter α/β of photons is a predictor for the sensitivity to LET changes. *Acta Oncologica* 52(3), 2013.

[42] A. Carabe-Fernandez et al. The incorporation of the concept of minimum RBE into the linear-quadratic model and the potential for improved radio- biological analysis of high-LET treatments. Int. J. *Radiation Biology* 83(1), 2007.

[43] T. Elsasser, M. Kramer, M. Scholz. Accuracy of the local effect model for the prediction of biologic effects of carbon ion beams in vitro and in vivo. Int. J. *Radiation Oncology* Biol. Phys. 71(3), 2008.

[44] G. Kraft, M. Scholz, and U. Bechthold. Tumor therapy and track structure. *Radiation and Environmental Biophysics*, 38:229{237, 12 1999. doi: 10.1007/ s004110050163.

[45] Y. Kase et al. Microdosimetric Measurements and Estimation of Human Cell Survival for Heavy-Ion Beams. *Radiation Research* 166, 2006.

[46] D. J. Carlson, R. D. Stewart, V. A. Semenenko, and G. A. Sandison. Combined use of Monte Carlo DNA damage simulations and deterministic repair models to examine putative mechanisms of cell killing. *Radiation Research*, 169:447{459, 04 2008. doi: 10.1667/rr1046.1.

[47] M. C. Frese, V. K. Yu, R. D. Steward, and D. J. Carlson. *International Journal of Radiation Oncology*Biology*Physics*, 83:44 2{ 450,2012. doi: 10.1016/ j.ijrobp.2011.06.1983.

[48] L. Polster et al. Extension of TOPAS for the simulation of proton radiation effects considering molecular and cellular endpoints. *Phys. Med. Biol.* 60(13), 2015.

[49] Y. Kase, T. Kanai, N. Matsufuji, Y. Furusawa, T. Elsasser, and M. Scholz. Biophysical calculation of cell survival probabilities using amorphous track structure models for heavy-ion irradiation. *Physics in Medicine and Biology*, 53:37{59, 01 2008. doi: 10.1088/0031-9155/53/1/003.

[50] McKeown SR. Defining normoxia, physoxia and hypoxia in tumours-implications for treatment response. Br J Radiol. (2014) 87:20130676. doi: 10.1259/bjr.20130676.

[51] J. Ramos-Méndeza,1, N. Domínguez-Kondob, J. Schuemannc, A. McNamarac, E. Moreno-Barbosab, Bruce Faddegona. LET-Dependent Intertrack Yields in Proton Irradiation at Ultra-High Dose Rates Relevant for FLASH Therapy. *Radiat Res.* 2020 October 02; 194(4): 351–362. doi:10.1667/RADE-20-00084.1.

[52] unife.it/medicina/radiologiamedica/insegnamenti/ cittanti-2018-19-colori/rb-2018-19-lezione-4

[53] K. Petersson, G. Adrian, K. Butterworth and S. J. McMahon. A Quantitative Analysis of the Role of Oxygen Tension in FLASH Radiation Therapy. *International Journal of Radiation Oncology, biology, phisics*.

[54] W. K. Hastings. Monte Carlo sampling methods using Markov chains and their applications, *Biometrika*, 1970, pp. 97-109.

[55] G A P Cirrone, PhD - INFN-LNS – Slides.

[56] International Conference on Computing in High Energy and Nuclear Physics 2012 (CHEP2012) IOP Publishing Journal of Physics: Conference Series 396 (2012) 022024 doi:10.1088/1742-6596/396/2/022024.

[57] Agostinelli S et al. 2003 Nucl. Instrum, and Methods A506 250-303.

[58] S. Incerti, G. Baldacchino et al. The GEANT4-DNA Project. *International Journal of Modeling, Simulation and Scientific Computing* Vol. 1, No. 2 (2010) 157–178. World Scientific Publishing Company. DOI: 10.1142/S1793962310000122

[59] Youfang Lai, Xun Jia and Yujie Chi. A new open-source GPU-based microscopic Monte Carlo simulation tool for the calculations of DNA damages caused by ionizing radiation --- Part I: Core algorithm and validation.

[60] gMicroMC: Accelerating Microscopic Monte Carlo Simulation Using Rapid Parallel Processing Platforms. Zhen Tian, Nan Qin, Min Yu Tsai, Steve Jiang, Xun Jia zhen.tian@utsouthwestern.edu

[61] Min-Yu Tsai, Youfang Lai, Yujie Chi, Xun Jia, and Shih-Hao Hung. 2020. Performance Evaluation of a GPU-based Monte Carlo Simulation Package for Water Radiolysis with sub-MeV Electrons. In International Conference on Research in Adaptive and Convergent Systems (RACS '20), October 13– 16, 2020, Gwangju, Republic of Korea. ACM, New York, NY, USA, 8 pages. https://doi.org/10.1145/3400286.3418241

[62] https://github.com/utaresearch/gMicroMC#readme

[63] Studying the oxygen effect in proton therapy via gpu-based microscopic Monte Carlo simulation by Marcos Joseph Guillen.

[64] Youfang Lai, Xun Jia and Yujie Chi. A new open-source GPU-based microscopic Monte Carlo simulation tool for the calculations of DNA damages caused by ionizing radiation — Part II: sensitivity and uncertainty analysis.

[65] Zhen Tian, Steve B. Jiang, and Xun Jia. Accelerated Monte Carlo Simulation on the Chemical Stage in Water Radiolysis using GPU. *Phys Med* Biol. 2017 April 21; 62(8): 3081–3096. doi:10.1088/1361-6560/aa6246.

[66] H. Nikjoo, P. O'Neill, D. T. Goodhead and M. Terrisol. Computational modelling of low-energy electron-induced DNA damage by early physical and chemical events. int. j. radiat. biol 1997, vol. 71, no. 5, 467± 483